Analysis of heterogeneous structures described by the two-temperature model

Stefano Giordano, Fabio Manca

▶ **To cite this version:**

Stefano Giordano, Fabio Manca. Analysis of heterogeneous structures described by the two-temperature model. International Journal of Heat and Mass Transfer, 2014, 78, pp.189-202. ⟨10.1016/j.ijheatmasstransfer.2014.06.074⟩. ⟨hal-01044787⟩

HAL Id: hal-01044787

https://hal.science/hal-01044787v1

Submitted on 18 Aug 2022

HAL is a multi-disciplinary open access archive for the deposit and dissemination of scientific research documents, whether they are published or not. The documents may come from teaching and research institutions in France or abroad, or from public or private research centers.

L'archive ouverte pluridisciplinaire **HAL**, est destinée au dépôt et à la diffusion de documents scientifiques de niveau recherche, publiés ou non, émanant des établissements d'enseignement et de recherche français ou étrangers, des laboratoires publics ou privés.

Distributed under a Creative Commons CC BY-NC 4.0 - Attribution - Non-commercial use - International License

Analysis of heterogeneous structures described by the two-temperature model

Stefano Giordano *, Fabio Manca

Joint International Laboratory LIA LEMAC/LICS, Institute of Electronics, Microelectronic and Nanotechnology (UMR CNRS 8520), PRES University North of France, Ecole Centrale de Lille, Avenue Poincaré, CS 60069, 59652 Villeneuve d'Ascq Cedex, France

We consider the homogenization problem for composite structures described by the two-temperature model of heat conduction. Our theory is based on the most general solutions of the standard two-temper-ature equations for the spherical geometry. This methodology allows us to thoroughly analyse different configurations. In particular, we prove two equivalence theorems for homogeneous and composite (core–shell structure) two-temperature spheres, which paradigmatically represent particles dispersed in standard particulate materials. As a matter of fact, the core–shell structure is essential to model inter-face deficiencies such as mixing phenomena and imperfect transport conditions at the particle–matrix contact surface. Then, we take into consideration a dispersion of particles and we examine the effects of the interfaces characterized by mixing and imperfect transport phenomena. We also discuss in detail the scale effects in heterogeneous systems composed of two-temperature components. The results here established can be used for designing and improving materials or, conversely, for interpreting experimental data in terms of the thermal behavior of their constituents.

1. Introduction

The determination of the effective properties of heterogeneous media is an important active field in material science with relevant applications in modern technology [1,2]. Many exact and approximated methodologies have been developed and used to understand the electric, magnetic, thermal and elastic response of composite systems and structures [3,4].

From the historical point of view, the seminal work of Maxwell represents the first attempt to analyse the electric conductivity of dilute dispersions of spheres embedded in a different matrix [5]. Subsequently, the dielectric properties of dispersions of ellipsoids were studied by Fricke [6] in order to model the response of some biological tissues. Further, several generalizations, e.g. to non-dilute configurations, were obtained through the differential method [7,8] and the multipole technique [9,10]. Also the nonlinear case has been largely analysed. Such studies find important applications in the intrinsic optical bistability [11], in the second and third harmonic generation [12] and in the mechanical characterization of nanocomposites [13]. Homogenization techniques have been proposed for populations of nonlinear particles embedded in a linear matrix as well [14,15].

An interesting approach, based on the equivalent inclusion method, has been developed in the framework of the steady-state thermal conduction [16]. This technique has been successfully used to determine the effective thermal conductivity of misoriented short fiber composites [17] and coated filler composites [18]. Further, the physical characterization of several complex materials has been performed by means of the so-called depolarization tensor [19–21]. More recently, a full anisotropic analysis has been conducted for elliptic [22] and ellipsoidal [23] particles and for parallel or random dispersions of cracks [24]. Current results concern anisotropic layered media with microinclusions [25], networks of uniform cylindrical particles [26], and the dynamic analysis of thermoelastic composites [27].

An important point in any effective medium theory concerns the presence of imperfect interfaces between the constituents of composite materials. Indeed, in many real cases of technological interest (especially at the nanoscale), the specific properties of real contacts among different phases play a crucial role, being often at the origin of the scale effects [28]. In recent literature two interface models have been proposed for describing two different limiting situations. The first zero thickness model is called *low conducting interface* and it is based on the so-called Kapitza resistance [29]. On the other hand, the second model, called *high conducting interface*, concerns the case of an interphase of very high conductivity with vanishing thickness. Several investigations on heterogeneous

* Corresponding author. Tel.: +33 3 20 19 79 58; fax: +33 3 20 19 79 84.
E-mail address: Stefano.Giordano@iemn.univ-lille1.fr (S. Giordano).

Nomenclature

a and b	phases of the two-temperature model
$\vec{J}_a$ and $\vec{J}_b$	heat fluxes in phases a and b
V_a and V_b	temperatures in phases a and b
k	coupling coefficient
σ_a and σ_b	thermal conductivities in phases a and b
$h = \sqrt{k(1/\sigma_a + 1/\sigma_b)}$	modified coupling parameter
$1/h$	coupling length
$Y_{nm}(\vartheta, \varphi)$	spherical harmonics
$P_n^m(\xi)$	associated Legendre polynomials
$\mathrm{i}_n(z)$and $\mathrm{k}_n(z)$	modified spherical Bessel functions
$I_\nu(z)$ and $K_\nu(z)$	modified cylindrical Bessel functions
Σ_a, Σ_b, and Σ_{ab}	equivalent conductivities
$\sigma_{a,eff}, \sigma_{b,eff}$, and k_{eff}	effective parameters
$c = R_2^3/R_1^3$	volume fraction of the core in the composite sphere
R_1 and R_2	shell and core radii
ϕ	volume fraction of the dispersed particles

materials with low [30–39] or high [33,37,39–42] conducting interfaces can be found in literature. Recent results concern the integration of the low and high interface paradigms in more general models based on the T and Π lattice structures [43,44] and theories for composites with curvilinearly anisotropic coated inclusions [45].

An aspect rarely taken into consideration in the analyses of heterogeneous materials is the two-temperature (or double-conductivity) behavior of components. For example, to model the thermal transport in metals this technique is largely utilised. In order to conveniently include the electron–phonon coupling, it is useful to designate electrons and phonons as two interacting subsystems with two different temperatures. This approach has been introduced and validated by observing the electron–phonon relaxation in metals after short laser pulses, used as ultrafast heating sources [46–49]. Further, this method has been applied to analyse the coupling properties of electrons and phonons at metal–dielectric interfaces [50,51] and efficiently implemented within two-temperature molecular dynamics simulations [52,53].

The same approach is usually applied to model the heat transfer in porous media [54]. The two constituents (solid porous structure and filling fluid) are described through two temperature fields, pertinent to a couple of effective macroscopic continua. Their interaction is often introduced by means of a linear term proportional to the temperature difference. This model can be directly introduced through phenomenological arguments, or it can be derived from coarse-graining or homogenization procedures of the real microstructure [55,56]. Anyway, the consideration of two different temperature fields is crucial for situations where the local thermal equilibrium is not valid. This corresponds to the so-called local thermal non-equilibrium assumption (LTNE). The methodology has been largely applied to different situations ranging from impulsive conduction in porous media [57] to fluid-porous interfaces [58]. Recently, a detailed analysis of the correspondence between one- and two-equation models for transport in heterogeneous porous media has been performed [59]. Here, a time nonlocal two-equation model, a time local two-equation model and one-equation time-asymptotic formulation have been thoroughly compared. It is interesting to observe that the thermal behavior of metals (electrons + phonons) and trabecular or porous materials (solid + fluid) can be modeled with the same formalism although the underlying physical phenomena take place at completely different length-scales.

Some studies have been recently published concerning the effective behavior of heterogeneous systems with phases described by the two-temperature model. The effects of the double-conductivity behavior have been elucidated in metal–nonmetal multilayers [60] and in metallic bilayers [61]. Moreover, an effective medium theory, consisting in a generalization of the Maxwell approach [5], has been presented for a dispersion of two-temperature particles embedded in a single-temperature matrix [62]. However, this problem has been investigated only under specific conditions. In particular, the combination of the mixing between the two conduction processes at the interface and the imperfect transport properties of the same interface has been neglected. In this paper, we approach the problem of homogenizing composite structures with two-temperature components (e.g. metals or porous materials) by taking into account all these complex interface phenomena. To do this, we start our analysis in Section 2 by obtaining the most general solutions of the standard double-conductivity equations for an arbitrary spherical geometry. These solutions allow us to analyse several configurations. In Section 3, we consider the behavior of a spherical two-temperature particle embedded in a different two-temperature matrix. We suppose to apply a uniform heat flow and we determine the temperature perturbations both inside and outside the particle. We therefore explain the non-uniformity of the temperature gradients within the particle and we describe the scale effects underlying the behavior of this system. In Section 4, we prove a first equivalence theorem concerning a homogeneous two-temperature particle embedded in a standard single-temperature matrix. In Section 5, we prove a second equivalence theorem dealing with an heterogeneous particle composed of a two-temperature core and a two-temperature external shell. This structure is essential to model the mixing phenomena and the imperfect transport at any interface. In fact, the external shell may be considered as a thin coating mimicking all the interface properties. Importantly enough, this approach can be also iteratively applied to homogenize a multi-coated particles composed of an arbitrary number of two-temperature layers. Finally, in Section 6, we take into consideration a dispersion of particles and we thoroughly examine the effects of the interfaces characterized by the above discussed defects (arbitrary mixing and imperfect transport). Furthermore, we also obtain and discuss the scale effects in heterogeneous systems composed of two-temperature components.

2. Formalism

We introduce the concept of the two-temperature model for the thermal conduction in metals and in trabecular or porous structures, the corresponding equations and the general solution for the spherical geometry. In these systems, two temperature fields are considered to describe the conduction phenomena within two different phases a and b (electrons and phonons in metals or the two constituents in saturated/stagnant porous media). The necessity of a double description is related to the possible lack of thermal equilibrium between the phases. Therefore, we define two thermal fluxes $\vec{J}_a$ and $\vec{J}_b$ in the two-temperature material. We underline that, also in stationary conditions, the local thermal non-equilibrium can be verified due to the heterogeneity of the system (presence of interfaces), described by specific boundary conditions. Transient processes and source terms, generating local thermal non-equilibrium as well, are not considered in this work. Moreover, it has been proved that upscaling in porous media yields

advective terms at the macroscale even when there is no advection at the microscale [56]. However, we also neglect here all transport phenomena described by advective terms. Anyway, in stationary conditions and without coupling between the conduction processes in a and b we would have $\vec{\nabla}\cdot\vec{J}_a = 0$ and $\vec{\nabla}\cdot\vec{J}_b = 0$, stating the energy conservation in each independent phase. In our model we introduce a local heat transfer between the constituents a and b controlled by a coupling coefficient k (see Fig. 1 where a porous microstructure is shown). We can therefore write

$$\vec{\nabla}\cdot\vec{J}_a - k(V_b - V_a) = 0, \tag{1}$$

$$\vec{\nabla}\cdot\vec{J}_b - k(V_a - V_b) = 0, \tag{2}$$

where V_a and V_b represent the temperatures of phases a and b, respectively (in general, they are the potentials of the transport process). The overall energy conservation is now confirmed by the relation $\vec{\nabla}\cdot(\vec{J}_a + \vec{J}_b) = 0$ (stationary regime). Moreover, we assume two linear constitutive equations $\vec{J}_a = \sigma_a\vec{E}_a = -\sigma_a\vec{\nabla}V_a$ and $\vec{J}_b = \sigma_b\vec{E}_b = -\sigma_b\vec{\nabla}V_b$ for the phases and, therefore, we obtain the couple of equations

$$\sigma_a\nabla^2 V_a + k(V_b - V_a) = 0, \tag{3}$$

$$\sigma_b\nabla^2 V_b + k(V_a - V_b) = 0. \tag{4}$$

We remark that the parameters σ_a, σ_b and k have been taken into account as known quantities in this context and, therefore, we have not considered their dependence on the actual volume fractions and microstructure of the phases a and b. However, the problem of linking the *axiomatic* two-temperature formalism with realistic two-phase assemblages has been largely approached in literature and the expressions of the three parameters σ_a, σ_b and k in terms of the microstructure description and the volume fraction values have been provided in several forms (see e.g. [55,56]).

By combining Eqs. (3) and (4) we have the uncoupled results

$$\nabla^2\nabla^2 V_a - k\left(\frac{1}{\sigma_a} + \frac{1}{\sigma_b}\right)\nabla^2 V_a = 0, \tag{5}$$

$$\nabla^2\nabla^2 V_b - k\left(\frac{1}{\sigma_a} + \frac{1}{\sigma_b}\right)\nabla^2 V_b = 0. \tag{6}$$

It means that the functions $\nabla^2 V_a - h^2 V_a$ and $\nabla^2 V_b - h^2 V_b$ are harmonic everywhere, where we have defined the parameter $h = \sqrt{k(1/\sigma_a + 1/\sigma_b)}$. We remark that the transformation of two-temperature models into two uncoupled equations has been performed in previous works. For instance, Vadasz [63] proposed and resolved a paradox concerning heat conduction in porous media subject to lack of thermal equilibrium by means of this technique. Moreover, he worked with the complete time varying equations. It is also interesting to point-out that the two-temperature model (taking into account non-stationary processes) is mathematically equivalent to the dual-phase-lagging model, as shown in Ref. [64].

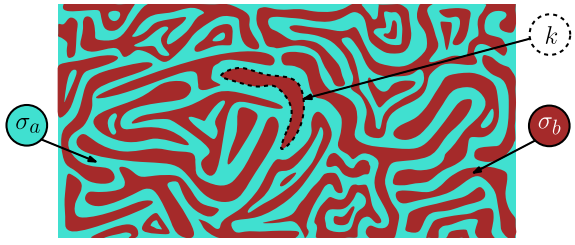

Fig. 1. Example or trabecular or porous structure composed of two distinct media with conductivities σ_a and σ_b connected with a coupling coefficient k. The thermal behavior is described by Eqs. (3) and (4).

The authors, to prove this equivalence, introduce uncoupled equations similar to Eqs. (5) and (6). This is a relevant result since all analytical solutions, obtained for the dual-phase-lagging model [65], can be directly applied to study two-phase systems, and vice-versa.

We search now for the general solution of Eqs. (3) and (4) for systems that can be described by spherical coordinates. To begin, we determine the first potential V_a. So, by using the general form of an harmonic function in standard spherical coordinates (r, ϑ, φ), we must consider the following nonhomogeneous equation ($\nabla^2 V_a - h^2 V_a$ is harmonic as stated in Eq. (5))

$$\nabla^2 V_a - h^2 V_a = \sum_{n=0}^{\infty}\sum_{m=-n}^{+n}\left(B_{nm}r^n + \frac{C_{nm}}{r^{n+1}}\right)Y_{nm}(\vartheta,\varphi), \tag{7}$$

where the spherical harmonics $Y_{nm}(\vartheta,\varphi)$ are defined (for $n \geqslant 0, -n \leqslant m \leqslant n$) as [66–68]

$$Y_{nm}(\vartheta,\varphi) = \sqrt{\frac{2n+1}{4\pi}\frac{(n-m)!}{(n+m)!}}P_n^m(\cos\vartheta)e^{im\varphi}, \tag{8}$$

and where $P_n^m(\xi)$ are the associated Legendre polynomials [66–68]

$$P_n^m(\xi) = (-1)^m(1-\xi^2)^{\frac{m}{2}}\frac{1}{2^n n!}\frac{d^{n+m}}{d\xi^{n+m}}\left(\xi^2-1\right)^n. \tag{9}$$

Eq. (7) is nonhomogeneous with the source term on the right hand side that is a linear combination of spherical harmonics. Therefore, we try to find a solution of the form $V_a = \sum_{n=0}^{\infty}\sum_{m=-n}^{+n} V_{nm}(r)Y_{nm}(\vartheta,\varphi)$. From now on we use the implicit notation for sums: $\sum_{n=0}^{\infty}\sum_{m=-n}^{+n}$ is understood for repeated indices n and m. We can determine the Laplacian of V_a as

$$\nabla^2 V_a = \frac{1}{r^2}\frac{\partial}{\partial r}\left(r^2\frac{\partial V_{nm}}{\partial r}\right)Y_{nm} + \frac{1}{r^2}V_{nm}\nabla_s^2 Y_{nm}, \tag{10}$$

where ∇_s^2 is the surface Laplacian operator for the unit sphere

$$\nabla_s^2 f = \frac{1}{\sin\vartheta}\frac{\partial}{\partial\vartheta}\left[\sin\vartheta\frac{\partial f}{\partial\vartheta}\right] + \frac{1}{\sin^2\vartheta}\frac{\partial^2 f}{\partial\varphi^2}. \tag{11}$$

We can use the following property

$$\nabla_s^2 Y_{nm} = -n(n+1)Y_{nm}, \tag{12}$$

stating that the spherical harmonics Y_{nm} are eigenfunctions of the surface Laplacian operator with eigenvalues $-n(n+1)$ [66]. We finally obtain the explicit form of the Laplacian of V_a as

$$\nabla^2 V_a = \frac{1}{r^2}\frac{\partial}{\partial r}\left(r^2\frac{\partial V_{nm}}{\partial r}\right)Y_{nm} - \frac{n(n+1)}{r^2}V_{nm}Y_{nm}. \tag{13}$$

Since the set of spherical harmonics represents a basis for the scalar functions defined on a spherical surface, from Eq. (7) we obtain an ordinary differential equation for the coefficients V_{nm}

$$\frac{1}{r^2}\frac{\mathrm{d}}{\mathrm{d}r}\left(r^2\frac{\mathrm{d}V_{nm}}{\mathrm{d}r}\right) - \frac{n(n+1)}{r^2}V_{nm} - h^2 V_{nm} = B_{nm}r^n + \frac{C_{nm}}{r^{n+1}}, \tag{14}$$

or, equivalently,

$$\frac{\mathrm{d}^2 V_{nm}}{\mathrm{d}r^2} + \frac{2}{r}\frac{\mathrm{d}V_{nm}}{\mathrm{d}r} - \left[n(n+1) + r^2h^2\right]\frac{V_{nm}}{r^2} = B_{nm}r^n + \frac{C_{nm}}{r^{n+1}}. \tag{15}$$

We remark that in Eqs. (14) and (15) no implicit sums must be taken into account. The associated homogeneous equation (with $B_{nm} = 0$ and $C_{nm} = 0$) is directly solved by the modified spherical Bessel functions $\mathsf{i}_n(z)$ and $\mathsf{k}_n(z)$. They can be defined through the modified cylindrical Bessel functions $I_\nu(z)$ and $K_\nu(z)$ [69]

$$\mathsf{i}_n(z) = \sqrt{\frac{\pi}{2z}}I_{n+\frac{1}{2}}(z), \quad \mathsf{k}_n(z) = \sqrt{\frac{\pi}{2z}}K_{n+\frac{1}{2}}(z), \tag{16}$$

or directly in terms of elementary functions [69]

$$\mathrm{i}_n(z) = z^n \left(\frac{1}{z}\frac{\mathrm{d}}{\mathrm{d}z}\right)^n \frac{\sinh z}{z}, \tag{17}$$

$$\mathrm{k}_n(z) = (-1)^n \frac{\pi}{2} z^n \left(\frac{1}{z}\frac{\mathrm{d}}{\mathrm{d}z}\right)^n \frac{\exp(-z)}{z}. \tag{18}$$

Anyway, the solution of the homogeneous equation associated to Eq. (15) is given by

$$V_{nm}^{\mathrm{h}} = a_{nm}\mathrm{i}_n(hr) + b_{nm}\mathrm{k}_n(hr), \tag{19}$$

where a_{nm} and b_{nm} are coefficients to be determined. In Appendix A we prove that the following expression represents a particular solution for the nonhomogeneous version of Eq. (15)

$$V_{nm}^{\mathrm{p}} = -\frac{1}{h^2}\left(B_{nm}r^n + \frac{C_{nm}}{r^{n+1}}\right). \tag{20}$$

Hence, the general solution is given by

$$\begin{aligned} V_{nm} &= V_{nm}^{\mathrm{h}} + V_{nm}^{\mathrm{p}} \\ &= a_{nm}\mathrm{i}_n(hr) + b_{nm}\mathrm{k}_n(hr) - \frac{1}{h^2}\left(B_{nm}r^n + \frac{C_{nm}}{r^{n+1}}\right). \end{aligned} \tag{21}$$

In order to write the final solutions for V_a and V_b in a symmetrical form it is convenient to define $\alpha_{nm} = \sigma_a a_{nm}, \beta_{nm} = \sigma_a b_{nm}, \gamma_{nm} = -\frac{1}{h^2}B_{nm}$ and $\delta_{nm} = -\frac{1}{h^2}C_{nm}$. These four sets of coefficients must be determined with the boundary conditions pertinent to the specific problem under consideration. We simply obtain

$$V_a(r,\vartheta,\varphi) = \left[\frac{1}{\sigma_a}\alpha_{nm}\mathrm{i}_n(hr) + \frac{1}{\sigma_a}\beta_{nm}\mathrm{k}_n(hr) + \gamma_{nm}r^n + \frac{\delta_{nm}}{r^{n+1}}\right]Y_{nm}(\vartheta,\varphi), \tag{22}$$

$$V_b(r,\vartheta,\varphi) = \left[-\frac{1}{\sigma_b}\alpha_{nm}\mathrm{i}_n(hr) - \frac{1}{\sigma_b}\beta_{nm}\mathrm{k}_n(hr) + \gamma_{nm}r^n + \frac{\delta_{nm}}{r^{n+1}}\right]Y_{nm}(\vartheta,\varphi). \tag{23}$$

These expressions represent the most general solution of Eqs. (3) and (4) in spherical coordinates. While the first expression has been determined by solving directly Eq. (5), the second one has been easily found through Eq. (3) solved for V_b. Eqs. (22) and (23) can be used to represent the general solution in a region comprised between two spherical surfaces (a spherical shell). For obtaining the regular solution inside a sphere we have to set $\beta_{nm} = 0$ and $\delta_{nm} = 0$ (the functions $\mathrm{k}_n(hr)$ and $\frac{1}{r^{n+1}}$ being singular for $r = 0$). On the other hand, for obtaining the regular solution outside a sphere we have to set $\alpha_{nm} = 0$ and $\gamma_{nm} = 0$ (the functions $\mathrm{i}_n(hr)$ and r^n being singular at infinity). In the following Sections we adopt these solutions to analyse some heterogeneous structures.

Some comments follow about the possible generalization of our technique to more refined models. It is possible to consider the transient behavior of the system by strongly complicating the mathematics of the problem. Indeed, if we take into account the transient terms of the heat equation with a permanent sinusoidal regime, the coefficient k in Eqs. (3) and (4) is transformed in a 2 by 2 matrix with complex entries. Then, we can envisage a similar development, but the arguments of the pertinent special functions become complex, involving several complications. Moreover, the consideration of advection or source terms is not possible with this formalism. Also the contemplation of nonlinear behaviors is prohibitive. As discussed in next sections, the temperature gradient inside two-temperature spherical particles is typically non uniform, making very difficult any nonlinear generalization. Only when the internal gradients are uniform (or quite uniform), the linear homogenization procedures can be generalized with nonlinear constitutive equations (see, e.g. [14,23,70]).

3. Spherical defect in a uniform heat flow

We consider an homogeneous material described by the two-temperature model with parameters σ_a, σ_b and k. If we take into consideration the simple case with $\vec{J}_a$ and $\vec{J}_b$ uniform and both parallel to the z-axis (uniform fluxes imposed in the whole considered space), we must have $V_a = -(J_a/\sigma_a)z$ and $V_b = -(J_b/\sigma_b)z$. These expressions can be easily derived from the linear constitutive equations $\vec{J}_a = -\sigma_a\vec{\nabla}V_a$ and $\vec{J}_b = -\sigma_b\vec{\nabla}V_b$. Since we also have $\nabla^2 V_a = 0$ and $\nabla^2 V_b = 0$ (the Laplacian of linear functions of x, y and z is always zero), we gather from Eqs. (3) and (4) that $V_a = V_b$ or, equivalently that $J_a/\sigma_a = J_b/\sigma_b$. It means that, if we impose uniform fluxes in the whole three-dimensional space, the stationary and homogeneous two temperature model forces the relation $J_a/\sigma_a = J_b/\sigma_b$ between the fluxes to be self-consistent. In this case we also observe that the total thermal flux $\vec{J}$ is given by $\vec{J} = -(\sigma_a + \sigma_b)\vec{\nabla}V$ (where $V = V_a = V_b$): it means that the total conductivity of a homogeneous bulk material is given by the sum of the two conductivities of the constituents. It is a well known result for a metallic material where the total conductivity can be obtained by adding the conductivity of the phonons and that of the electrons.

We consider now a spherical defect embedded in a matrix where a uniform flux is present. We consider a two-temperature sphere with radius R and parameters σ_{a2}, σ_{b2} and k_2 embedded in a matrix with parameters σ_{a1}, σ_{b1} and k_1 (see Fig. 2 for details). As before, for both constituents we define $h_i = \sqrt{k_i(1/\sigma_{ai} + 1/\sigma_{bi})}$. The remote fields, corresponding to the uniform flux, will be described by $V_{a1} = V_{b1} = -Ez = -Er\cos\vartheta$ where $E = J_{a1}/\sigma_{a1} = J_{b1}/\sigma_{b1}$ is the applied temperature gradient. Since the remote potentials have the form $-Er\cos\vartheta$, the general solutions given in Eqs. (22) and (23) must be used only with the terms corresponding to $Y_{10}(\vartheta,\varphi) = \sqrt{\frac{3}{4\pi}}\cos\vartheta$. We finally assume these mathematical forms for the potentials:

$$V_{a2} = \left[\frac{\alpha}{\sigma_{a2}}\mathrm{i}_1(h_2 r) + \gamma r\right]\cos\vartheta, \tag{24}$$

$$V_{b2} = \left[-\frac{\alpha}{\sigma_{b2}}\mathrm{i}_1(h_2 r) + \gamma r\right]\cos\vartheta, \tag{25}$$

inside the spherical particle and

$$V_{a1} = \left[\frac{\beta}{\sigma_{a1}}\mathrm{k}_1(h_1 r) + \frac{\delta}{r^2} - Er\right]\cos\vartheta, \tag{26}$$

$$V_{b1} = \left[-\frac{\beta}{\sigma_{b1}}\mathrm{k}_1(h_1 r) + \frac{\delta}{r^2} - Er\right]\cos\vartheta, \tag{27}$$

outside it. To begin we consider the simplest boundary conditions for $r = R$, corresponding to the case without mixing of the fluxes $\vec{J}_a$ and $\vec{J}_b$ at the interface. Later on, we will discuss more complicated structures mimicking the mixing phenomena at the interface. So,

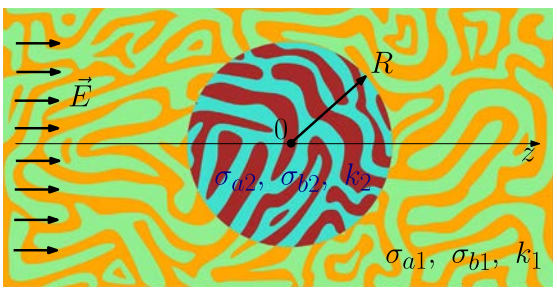

Fig. 2. Scheme of a spherical inhomogeneity of radius R embedded in a different matrix. Both phases are described by the two-temperature model.

we have $V_{a1}=V_{a2}, V_{b1}=V_{b2}, \sigma_{a1}\partial V_{a1}/\partial r=\sigma_{a2}\partial V_{a2}/\partial r$ and $\sigma_{b1}\partial V_{b1}/\partial r=\sigma_{b2}\partial V_{b2}/\partial r$ for $r=R$. These four conditions allow for the determination of the unknown coefficients α,β,δ and γ defined in Eqs. (24)–(27). After a very long but straightforward calculation we get

$$\alpha=\frac{\sigma_{a2}\sigma_{b2}(\sigma_{b1}\sigma_{a2}-\sigma_{a1}\sigma_{b2})}{(\sigma_{a2}+\sigma_{b2})^2}\frac{1}{\mathcal{D}\mathrm{i}_1(h_2R)}\frac{3E}{1+2\mathcal{F}+2\mathcal{Q}},$$
$$\beta=\frac{\sigma_{a1}\sigma_{b1}(\sigma_{b1}\sigma_{a2}-\sigma_{a1}\sigma_{b2})}{(\sigma_{a1}+\sigma_{b1})(\sigma_{a2}+\sigma_{b2})}\frac{1}{\mathcal{D}\mathrm{k}_1(h_1R)}\frac{3E}{1+2\mathcal{F}+2\mathcal{Q}},$$
$$\delta=ER^3\frac{1-\mathcal{F}-\mathcal{Q}}{1+2\mathcal{F}+2\mathcal{Q}},$$
$$\gamma=-E\frac{3\mathcal{F}}{1+2\mathcal{F}+2\mathcal{Q}}, \tag{28}$$

where

$$\mathcal{D}=\frac{k_2}{h_2}\frac{\mathrm{i}_1'(h_2R)}{\mathrm{i}_1(h_2R)}-\frac{k_1}{h_1}\frac{\mathrm{k}_1'(h_1R)}{\mathrm{k}_1(h_1R)},$$
$$\mathcal{F}=\frac{\sigma_{a1}+\sigma_{b1}}{\sigma_{a2}+\sigma_{b2}},$$
$$\mathcal{Q}=\frac{1}{R\mathcal{D}}\frac{(\sigma_{b1}\sigma_{a2}-\sigma_{a1}\sigma_{b2})^2}{(\sigma_{a1}+\sigma_{b1})(\sigma_{a2}+\sigma_{b2})^2}. \tag{29}$$

It is interesting to remark two important limiting cases of the above general solution: if $k_1=k_2=0$ there is no thermal coupling between a and b, both inside and outside the particle. Therefore, the two phases are independent and the inclusion behavior is described by the well-known Lorentz field for a spherical particle [5,8], i.e. by

$$V_{a2}=-\frac{3\sigma_{a1}}{2\sigma_{a1}+\sigma_{a2}}Er\cos\vartheta, \tag{30}$$
$$V_{b2}=-\frac{3\sigma_{b1}}{2\sigma_{b1}+\sigma_{b2}}Er\cos\vartheta, \tag{31}$$

representing uniform temperature gradients inside the particle, and by

$$V_{a1}=-\left[1+\frac{\sigma_{a1}-\sigma_{a2}}{2\sigma_{a1}+\sigma_{a2}}\left(\frac{R}{r}\right)^3\right]Er\cos\vartheta, \tag{32}$$
$$V_{b1}=-\left[1+\frac{\sigma_{b1}-\sigma_{b2}}{2\sigma_{b1}+\sigma_{b2}}\left(\frac{R}{r}\right)^3\right]Er\cos\vartheta, \tag{33}$$

representing the classical dipolar behavior outside it. Moreover, for $k_1\to\infty$ or $k_2\to\infty$ there is the strongest interaction between the phases and, accordingly, they exhibit the same behavior (thermal equilibrium), described by a particle of conductivity $\sigma_{t2}=\sigma_{a2}+\sigma_{b2}$ embedded in a matrix of conductivity $\sigma_{t1}=\sigma_{a1}+\sigma_{b1}$. The resulting temperature profiles are therefore given by

$$V_{a2}=V_{b2}=-\frac{3\sigma_{t1}}{2\sigma_{t1}+\sigma_{t2}}Er\cos\vartheta, \tag{34}$$

inside the particle, and by

$$V_{a1}=V_{b1}=-\left[1+\frac{\sigma_{t1}-\sigma_{t2}}{2\sigma_{t1}+\sigma_{t2}}\left(\frac{R}{r}\right)^3\right]Er\cos\vartheta, \tag{35}$$

outside it. Previous limits have been verified both theoretically, starting from Eqs. (24)–(27), and numerically, by plotting the temperature profiles, as shown in Fig. 3. Here, we considered the perturbations induced to the pre-existing linear temperature profile $V_{a1}=V_{b1}=-Er\cos\vartheta$, generated by the embedding of the particle; they are defined as

$$\Delta V_a=\begin{cases}V_{a2}+Er\cos\vartheta & \text{if } 0\leqslant r<1,\\ V_{a1}+Er\cos\vartheta & \text{if } r\geqslant 1,\end{cases} \tag{36}$$

and

$$\Delta V_b=\begin{cases}V_{b2}+Er\cos\vartheta & \text{if } 0\leqslant r<1,\\ V_{b1}+Er\cos\vartheta & \text{if } r\geqslant 1.\end{cases} \tag{37}$$

In Fig. 3 the limiting cases are represented as follows: Eqs. (30) and (32) correspond to the heavy cyan curves, Eqs. (31) and (33) to the heavy violet curves and, finally, Eqs. (34) and (35) to the heavy green curves. It is interesting to observe that for $h_1R\ll 1$ and $h_2R\ll 1$ we have a weak interaction between a and b or, equivalently, a small radius of the particle (nanoscale). In this case, we are far from the thermal equilibrium between the phases and we observe possible large deviations between V_a and V_b: the extreme situation corresponds to the couple of different Lorentz field given in Eqs. (30) and (31). On the other hand, if $h_1R\gg 1$ or $h_2R\gg 1$ we have a strong interaction between a and b or, equivalently, a large radius of the particle (macroscale). In this case, we are near the thermal equilibrium between the phases and therefore we have $V_a\sim V_b$: the extreme situation corresponds to the Lorentz field given in Eq. (34). It means that the parameters h_iR play a central role in assessing the scale effects in systems with spherical particles exhibiting the two-temperature behavior. In particular, it is important to remark that the local thermal equilibrium can be easily lost at the nanoscale, making crucial the use of the two-temperature model for modeling composite structures with small particles. Interestingly enough, we deduce, from Fig. 3a that for small values of k_1 (weak interaction in the matrix) we have strongly non-uniform temperature gradients within the particle. Similarly, we observe from Fig. 3b that small values of k_2 lead to quite uniform temperature gradients within the particle; this latter result is expected since negligible values of k_2 allow us to use standard solutions for a single-temperature particle, which are indeed characterized by linear temperature profiles. To conclude, from the comparison of Fig. 3a and b and Fig. 3c we draw the following result: to obtain the same Lorentz behavior for the two phases, as given in Eqs. (34) and(35) (strong coupling), it is sufficient to have only one of the two parameters k_1 and k_2 approaching infinity; on the contrary, for observing the separated and independent Lorentz curves given by Eqs. (30), (32) and (31), (33) we must impose both interaction coefficients to zero.

4. Equivalent conductivities of a homogeneous two-temperature sphere

We consider a homogeneous sphere described by the two-temperature model (parameters σ_a,σ_b,k and radius R). We suppose to embed this particle in a standard material having a single temperature description. To do this, we take into account three configurations characterized by three different boundary conditions. In the first case the external material is directly connected only to the phase a of the sphere (Fig. 4a), in the second case to the phase b (Fig. 4b) and, finally, in the third case to both phases a and b (Fig. 4c). For convenience, the conductivity of the matrix is named σ_{a0} in the first case, σ_{b0} in the second case and σ_0 in the third one.

In any case the solutions within the spherical particle are given by

$$V_a=\left[\frac{\alpha}{\sigma_a}\mathrm{i}_1(hr)+\gamma r\right]\cos\vartheta, \tag{38}$$
$$V_b=\left[-\frac{\alpha}{\sigma_b}\mathrm{i}_1(hr)+\gamma r\right]\cos\vartheta, \tag{39}$$

and the external potential (purely harmonic) is

$$V_{ext}=\left[-E_0r+\frac{\xi}{r^2}\right]\cos\vartheta, \tag{40}$$

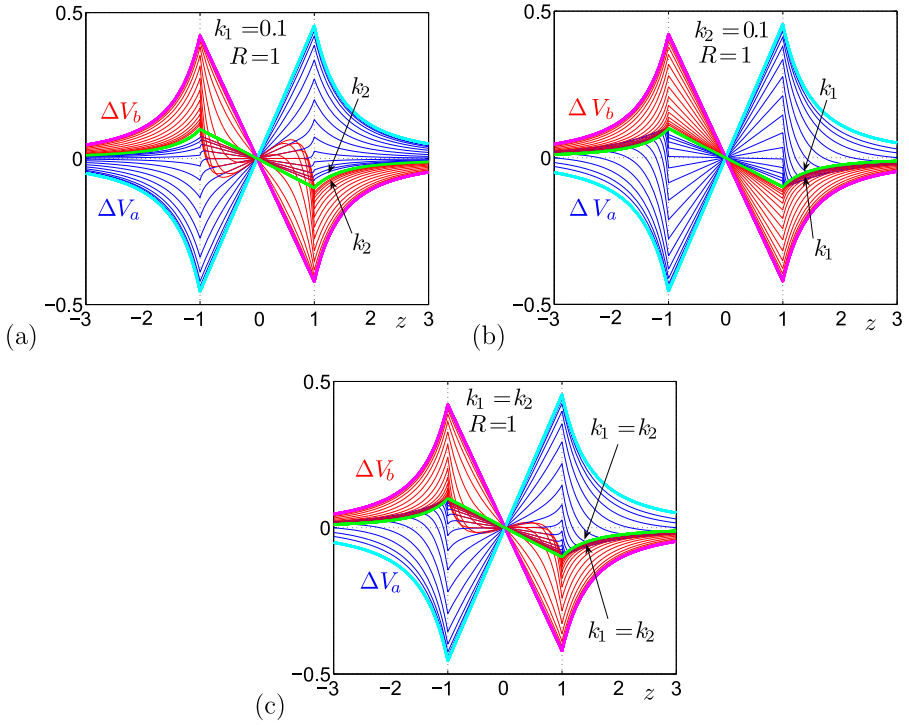

Fig. 3. Temperature perturbations ΔV_a and ΔV_b (evaluated on the z axis) induced by the introduction of the spherical defect: in the first case (a) we fixed $k_1 = 0.1$ and we varied k_2; in the second case (b) we considered $k_2 = 0.1$ and we varied k_1; finally, in the third case (c) we varied both constants, by maintaining $k_1 = k_2$. The varying quantities (arrows) always assume 15 equispaced values (in logarithmic scale) in the range $(10^0, 10^5)$. We considered everywhere the parameters $R = 1, E = 1, \sigma_{a1} = 10, \sigma_{a2} = 35, \sigma_{b1} = 45$ and $\sigma_{b2} = 5$ (in a.u.).

where E_0 represents the remotely applied temperature gradient. The boundary conditions follow:

$$V_a|_R = V_{ext}|_R, \quad \sigma_a \frac{\partial V_a}{\partial r}\bigg|_R = \sigma_{a0} \frac{\partial V_{ext}}{\partial r}\bigg|_R, \quad \frac{\partial V_b}{\partial r}\bigg|_R = 0 \tag{41}$$

for the first case,

$$V_b|_R = V_{ext}|_R, \quad \sigma_b \frac{\partial V_b}{\partial r}\bigg|_R = \sigma_{b0} \frac{\partial V_{ext}}{\partial r}\bigg|_R, \quad \frac{\partial V_a}{\partial r}\bigg|_R = 0 \tag{42}$$

for the second case and, finally,

$$V_a|_R = V_{ext}|_R, \quad V_b|_R = V_{ext}|_R, \quad \sigma_a \frac{\partial V_a}{\partial r}\bigg|_R + \sigma_b \frac{\partial V_b}{\partial r}\bigg|_R = \sigma_0 \frac{\partial V_{ext}}{\partial r}\bigg|_R \tag{43}$$

for the third one. For the three configurations we can straightforwardly find the unknown coefficients α, γ and ξ, by solving the corresponding linear system.

We have now to compare these results with the behavior of a single-temperature particle embedded in a single-temperature matrix. To do this, we consider a sphere with conductivity Σ embedded in a matrix with conductivity σ_m, and subjected to a uniform negative temperature gradient E_0 along the z-axis. Since the remote temperature has the form $-E_0 r\cos\vartheta$, the internal and external harmonic temperature perturbations $V_{int} + E_0 r\cos\vartheta = \sum_n \sum_m B_{nm} r^n Y_{nm}\ (\vartheta, \varphi)$ and $V_{ext} + E_0 r\cos\vartheta = \sum_n \sum_m C_{nm} r^{-n-1} Y_{nm}(\vartheta, \varphi)$ must contain only the terms proportional to $Y_{10}(\vartheta, \varphi) = \sqrt{\frac{3}{4\pi}}\cos\vartheta$. We therefore search the solutions in the form

$$V_{int} = [-E_0 r + \eta r]\cos\vartheta, \tag{44}$$

$$V_{ext} = \left[-E_0 r + \frac{\xi}{r^2}\right]\cos\vartheta, \tag{45}$$

where η and ξ are unknowns coefficients and we impose the boundary conditions forcing the continuity of the temperature $V_{int}|_R = V_{ext}|_R$ and of the heat flux $\Sigma \frac{\partial V_{int}}{\partial r}\big|_R = \sigma_m \frac{\partial V_{ext}}{\partial r}\big|_R$. Hence, we can easily solve the corresponding system of equations in the unknown coefficients η and ξ, eventually obtaining

$$\eta = \frac{\Sigma - \sigma_m}{\Sigma + 2\sigma_m} E_0, \tag{46}$$

$$\xi = \frac{\Sigma - \sigma_m}{\Sigma + 2\sigma_m} E_0 R^3. \tag{47}$$

Interestingly enough, the internal negative temperature gradient is given by $E_0 - \eta = 3\sigma_m E_0/(\Sigma + 2\sigma_m)$, which is the classical Lorentz field largely used in the electrostatic counterpart [5,8].

Since a homogeneous single temperature sphere with conductivity Σ embedded in a matrix with conductivity σ_m generates an external field (dipolar behavior) described by Eqs. (45) and (47), we simply obtain the exact equivalent conductivity of the two-temperature particle via the equation (inverse of Eq. (47)),

$$\Sigma = \frac{E_0 R^3 + 2\xi}{E_0 R^3 - \xi}\sigma_m, \tag{48}$$

where ξ is the solution of one of the three sets of conditions given in Eqs. (41)–(43) σ_m is given by σ_{a0}, σ_{b0} or σ_0 depending on the configuration considered. This procedure eventually leads to the following equivalent conductivities

$$\Sigma_a = \sigma_a \frac{1 + \frac{\sigma_a}{\sigma_b}}{\frac{1}{hR}\frac{i_1(hR)}{i_1'(hR)} + \frac{\sigma_a}{\sigma_b}}, \tag{49}$$

$$\Sigma_b = \sigma_b \frac{1 + \frac{\sigma_b}{\sigma_a}}{\frac{1}{hR}\frac{i_1(hR)}{i_1'(hR)} + \frac{\sigma_b}{\sigma_a}}, \tag{50}$$

$$\Sigma_{ab} = \sigma_a + \sigma_b. \tag{51}$$

We have therefore proved the *first theorem of equivalence*: a two-temperature sphere embedded in a single-temperature matrix can be substituted by an *ad-hoc* single-temperature particle having the conductivity given by Eqs. (49), (50) or (51), depending on the

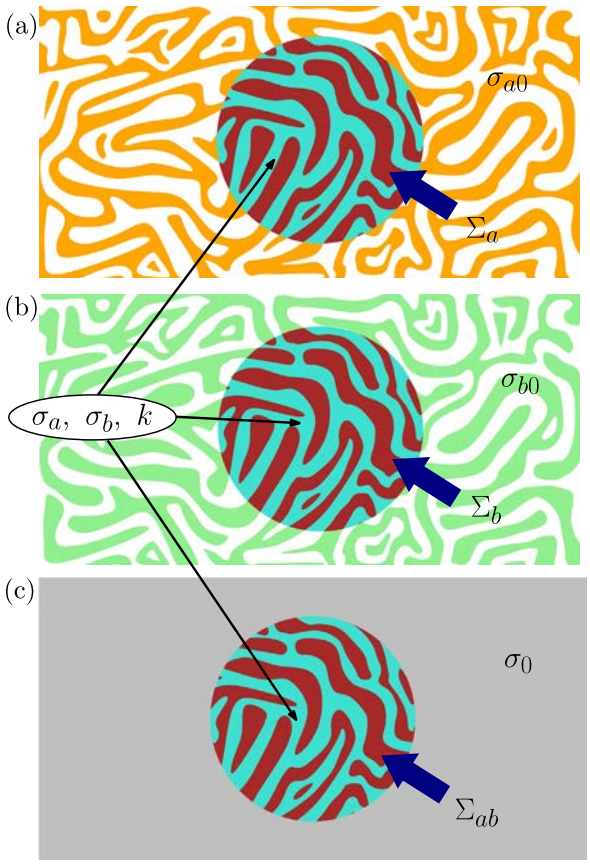

Fig. 4. Homogeneous two-temperature particle embedded in a single-temperature matrix. Three configurations correspond to the external material directly connected to the phase a of the sphere (a), to the phase b (b) and, finally, to both phases (c).

configuration considered. It is interesting to note the scale effects induced in Σ_a and Σ_b, represented by the explicit dependence on the particle radius R (through the dimensionless factor hR, already discussed in the previous Section). On the contrary, Σ_{ab} is simply given by the sum of the partial conductivities for the homogeneous particle. A more complex behavior will be studied for the heterogeneous particle in the next Section. An important point related to previous expressions is the following: the knowledge of the three equivalent conductivities Σ_a, Σ_b and Σ_{ab} is necessary and sufficient to have a complete characterization of the two-temperature particle response. To prove this statement we show that there is a biunivocal correspondence between $(\Sigma_a, \Sigma_b, \Sigma_{ab})$ and (σ_a, σ_b, k). To this aim, we define the following quantities

$$\mathcal{X}_a = \frac{\Sigma_{ab}}{\Sigma_a}, \quad \mathcal{X}_b = \frac{\Sigma_{ab}}{\Sigma_b}, \quad \omega = \frac{1}{hR}\frac{\mathrm{i}_1(hR)}{\mathrm{i}_1'(hR)}, \tag{52}$$

and we invert the system given in Eqs. (49)–(51), by obtaining σ_a, σ_b and ω

$$\sigma_a = \Sigma_{ab}\frac{\sqrt{\mathcal{X}_a - 1} - \sqrt{\mathcal{X}_b - 1}}{\mathcal{X}_a - \mathcal{X}_b}\sqrt{\mathcal{X}_b - 1}, \tag{53}$$

$$\sigma_b = \Sigma_{ab}\frac{\sqrt{\mathcal{X}_a - 1} - \sqrt{\mathcal{X}_b - 1}}{\mathcal{X}_a - \mathcal{X}_b}\sqrt{\mathcal{X}_a - 1}, \tag{54}$$

$$\omega = \sqrt{\mathcal{X}_a - 1}\sqrt{\mathcal{X}_b - 1}. \tag{55}$$

Moreover, we observe that the quantity ω is directly related to the coupling coefficient k (or, equivalently, to h). Indeed, if we define the function

$$f(z) = \frac{1}{z}\frac{\mathrm{i}_1(z)}{\mathrm{i}_1'(z)} = \frac{z\cosh z - \sinh z}{(z^2+2)\sinh z - 2z\cosh z}, \tag{56}$$

which is monotonically decreasing from 1 to 0 for $z > 0$, then we can find by inversion $hR = f^{-1}(\omega)$ and, since $h = \sqrt{k(1/\sigma_a + 1/\sigma_b)}$, we can also obtain the coupling coefficient

$$k = \frac{1}{R^2}\frac{1}{\frac{1}{\sigma_a}+\frac{1}{\sigma_b}}\left[f^{-1}\left(\sqrt{\mathcal{X}_a - 1}\sqrt{\mathcal{X}_b - 1}\right)\right]^2. \tag{57}$$

We remark that f^{-1} can not be written in closed form but it can be straightforwardly evaluated numerically. We have therefore proved the following statement: the knowledge of the three observable quantities Σ_a, Σ_b and Σ_{ab} is completely equivalent to the knowledge of the two-temperature model parameters σ_a, σ_b and k. This conclusion will be very useful to homogenize the composite sphere structure in the following Section.

5. Effective conductivities of a composite two-temperature sphere

We consider a composite sphere constituted by a core of radius R_2 and a shell of radius R_1, both described by the two-temperature model. We suppose to have the parameters σ_{a2}, σ_{b2} and k_2 inside the core and σ_{a1}, σ_{b1} and k_1 within the external shell. The aim of this section is to obtain an exact homogenization technique for this structure, leading to a two-temperature effective behavior of the composite sphere described by three parameters $\sigma_{a,eff}, \sigma_{b,eff}$ and k_{eff}. As already discussed in the Introduction, this model is useful to describe at least two important situations: (i) the external shell, if considered as a thin interphase, is able to take into consideration both the mixing processes between the two independent conduction phenomena (e.g. electrons and phonons in metals) at the interface (controlled by k_1) and the possible imperfect transport properties at the same interface (controlled by σ_{a1} and σ_{b1}) [50–52]; in this case the thin shell may represent the low conductivity model (Kapitza like) or the high conductivity model largely used for mimicking the lack of thermal continuity between particle and matrix [33,37]; (ii) an interesting application of such homogenization procedures concerns multi-shelled (or multi-coated) and graded two-temperature particles; by means of an iterative procedure we may recursively homogenize the whole structure allowing the substitution of a very complex double-conductivity system with a simpler homogeneous one.

In order to homogenize the composite particle, we determine the quantities Σ_a, Σ_b and Σ_{ab}, defined in previous Section, and then we use Eqs. (53), (54) and (57) to obtain the effective properties. As before, we suppose to embed the particle in a (single temperature) matrix with three different boundary conditions. In the first case the matrix is directly connected only to the phase a of the external shell (Fig. 5a), in the second case to the phase b of the external shell (Fig. 5b) and, finally, in the third case to both phases of the external shell (Fig. 5c). In any case the solutions inside the spherical core are given by

$$V_{a2} = \left[\frac{\alpha}{\sigma_{a2}}\mathrm{i}_1(h_2 r) + \gamma r\right]\cos\vartheta, \tag{58}$$

$$V_{b2} = \left[-\frac{\alpha}{\sigma_{b_2}}\mathrm{i}_1(h_2 r) + \gamma r\right]\cos\vartheta, \tag{59}$$

within the external shell can be written as

$$V_{a1} = \left[\frac{\tau}{\sigma_{a1}}\mathrm{i}_1(h_1 r) + \frac{\beta}{\sigma_{a1}}\mathrm{k}_1(h_1 r) + \rho r + \frac{\delta}{r^2}\right]\cos\vartheta, \tag{60}$$

$$V_{b1} = \left[-\frac{\tau}{\sigma_{b1}}\mathrm{i}_1(h_1 r) - \frac{\beta}{\sigma_{b1}}\mathrm{k}_1(h_1 r) + \rho r + \frac{\delta}{r^2}\right]\cos\vartheta, \tag{61}$$

and the external potential (purely harmonic) is

$$V_{ext} = \left[-E_0 r + \frac{\xi}{r^2}\right]\cos\vartheta. \tag{62}$$

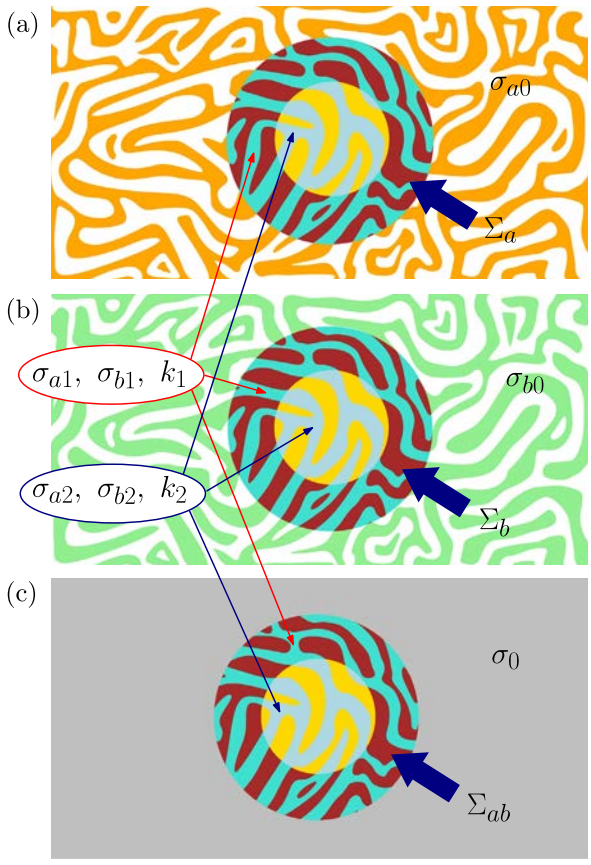

Fig. 5. Composite (core of radius R_2 in a shell of radius R_1) two-temperature particle embedded in a single-temperature matrix. Three configurations correspond to the matrix directly connected to the phase a of the external shell (a), to the phase b of the external shell (b) and, finally, to both phases of the shell (c).

The boundary conditions follow:

$$V_{a2}|_{R_2} = V_{a1}|_{R_2}, \quad \sigma_{a2}\frac{\partial V_{a2}}{\partial r}\bigg|_{R_2} = \sigma_{a1}\frac{\partial V_{a1}}{\partial r}\bigg|_{R_2},$$

$$V_{b2}|_{R_2} = V_{b1}|_{R_2}, \quad \sigma_{b2}\frac{\partial V_{b2}}{\partial r}\bigg|_{R_2} = \sigma_{b1}\frac{\partial V_{b1}}{\partial r}\bigg|_{R_2},$$

$$V_{a1}|_{R_1} = V_{ext}|_{R_1}, \quad \sigma_{a1}\frac{\partial V_{a1}}{\partial r}\bigg|_{R_1} = \sigma_{a0}\frac{\partial V_{ext}}{\partial r}\bigg|_{R_1},$$

$$\frac{\partial V_{b1}}{\partial r}\bigg|_{R_1} = 0 \tag{63}$$

for the first case,

$$V_{a2}|_{R_2} = V_{a1}|_{R_2}, \quad \sigma_{a2}\frac{\partial V_{a2}}{\partial r}\bigg|_{R_2} = \sigma_{a1}\frac{\partial V_{a1}}{\partial r}\bigg|_{R_2},$$

$$V_{b2}|_{R_2} = V_{b1}|_{R_2}, \quad \sigma_{b2}\frac{\partial V_{b2}}{\partial r}\bigg|_{R_2} = \sigma_{b1}\frac{\partial V_{b1}}{\partial r}\bigg|_{R_2},$$

$$V_{b1}|_{R_1} = V_{ext}|_{R_1}, \quad \sigma_{b1}\frac{\partial V_{b1}}{\partial r}\bigg|_{R_1} = \sigma_{b0}\frac{\partial V_{ext}}{\partial r}\bigg|_{R_1},$$

$$\frac{\partial V_{a1}}{\partial r}\bigg|_{R_1} = 0 \tag{64}$$

for the second case and, finally,

$$V_{a2}|_{R_2} = V_{a1}|_{R_2}, \sigma_{a2}\frac{\partial V_{a2}}{\partial r}\bigg|_{R_2} = \sigma_{a1}\frac{\partial V_{a1}}{\partial r}\bigg|_{R_2},$$

$$V_{b2}|_{R_2} = V_{b1}|_{R_2}, \sigma_{b2}\frac{\partial V_{b2}}{\partial r}\bigg|_{R_2} = \sigma_{b1}\frac{\partial V_{b1}}{\partial r}\bigg|_{R_2},$$

$$V_{a1}|_{R_1} = V_{ext}|_{R_1}, V_{b1}|_{R_1} = V_{ext}|_{R_1},$$

$$\sigma_{a1}\frac{\partial V_{a1}}{\partial r}\bigg|_{R_1} + \sigma_{b1}\frac{\partial V_{b1}}{\partial r}\bigg|_{R_1} = \sigma_0\frac{\partial V_{ext}}{\partial r}\bigg|_{R_1} \tag{65}$$

for the third one. Each of the systems defined in Eqs. (63)–(65) allows for the determination of the seven unknowns $\alpha, \gamma, \tau, \beta, \rho, \delta$ and ξ, defined in Eqs. (58)–(62). It can be done numerically or analytically, depending on the aim of the analysis conducted. Moreover, the three equivalent conductivities Σ_a, Σ_b and Σ_{ab} can be directly calculated through Eq. (48), where ξ is one of the parameters obtained from Eqs. (63)–(65) for the three configurations shown in Fig. 5, respectively. The explicit expressions for Σ_a, Σ_b and Σ_{ab} are very complicated and they do not provide further understanding beyond the numerical results described below. Hence, for the sake of brevity, these expressions are not reported here. In addition to the values Σ_a, Σ_b and Σ_{ab}, as above said, we can also numerically determine $\sigma_{a,eff}, \sigma_{b,eff}$ and k_{eff} through Eqs. (53), (54) and (57). In Fig. 6 we show the results for $k_1 = 0$ and $k_2 \neq 0$. Similarly, in Fig.7 we show the results for $k_2 = 0$ and $k_1 \neq 0$. In both cases we show the conductivities versus the volume fraction $c = R_2^3/R_1^3$ of the core in the entire range $(0, 1)$. Moreover, in Fig. 8 we considered the effective conductivities in terms of $k_1 \neq 0$ and $k_2 \neq 0$ for a fixed volume fraction $c = 0.4$. In all numerical calculations we assumed the parameters $R_1 = 1, \sigma_{a1} = 10, \sigma_{a2} = 35, \sigma_{b1} = 45$ and $\sigma_{b2} = 5$ in arbitrary units. In contrast with the previous Section, Eq. (51), we underline that the results for Σ_{ab} are now not trivial because of the heterogeneous structure of the particle.

It is interesting to observe that, for $k_1 = 0$ and $k_2 = 0$, the quantities Σ_a and $\sigma_{a,eff}$ converge to the Maxwell mixing rule [5]

$$\sigma_{Max,a} = \sigma_{a1}\frac{2\sigma_{a1} + \sigma_{a2} - 2c(\sigma_{a1} - \sigma_{a2})}{2\sigma_{a1} + \sigma_{a2} + c(\sigma_{a1} - \sigma_{a2})}, \tag{66}$$

represented by the heavy cyan curve in Figs. 6 and 7 (plots a and b). In the same way, always for $k_1 = 0$ and $k_2 = 0$, the quantities Σ_b and $\sigma_{b,eff}$ converge to the Maxwell mixing rule

$$\sigma_{Max,b} = \sigma_{b1}\frac{2\sigma_{b1} + \sigma_{b2} - 2c(\sigma_{b1} - \sigma_{b2})}{2\sigma_{b1} + \sigma_{b2} + c(\sigma_{b1} - \sigma_{b2})} \tag{67}$$

represented by the heavy violet curve in Figs. 6 and 7 (plots a and b). The link between our results and the Maxwell mixing rule can be further explained as follows. If we consider a structured sphere composed of a one-temperature core of conductivity σ_2 and a one-temperature shell of conductivity σ_1, embedded in a matrix of conductivity σ_m, and subjected to a uniform temperature gradient E_0, we can use the solutions

$$V_{int} = [-E_0 r + \eta r]\cos\vartheta \quad (0 < r < R_2), \tag{68}$$

$$V_{shell} = \left[-E_0 r + \rho r + \frac{\delta}{r^2}\right]\cos\vartheta \quad (R_2 < r < R_1), \tag{69}$$

$$V_{ext} = \left[-E_0 r + \frac{\xi}{r^2}\right]\cos\vartheta \quad (R_1 < r < +\infty), \tag{70}$$

to represent the temperature behavior in the whole space. By using the classical boundary conditions imposing the continuity of the temperature and the continuity of the heat flux over the spherical surface of radius R_1 and R_2, it is straightforward to determine the unknown coefficient η, ρ, δ and ξ. Thus, the knowledge of ξ, corresponding to the external response of the overall composite particle, allows us to obtain the effective conductivity of the particle via the expression $\sigma_{Max} = \frac{E_0 R_1^3 + 2\xi}{E_0 R_1^3 - \xi}\sigma_m$ (see Eq. (48)). After simple but long calculations we can obtain the result

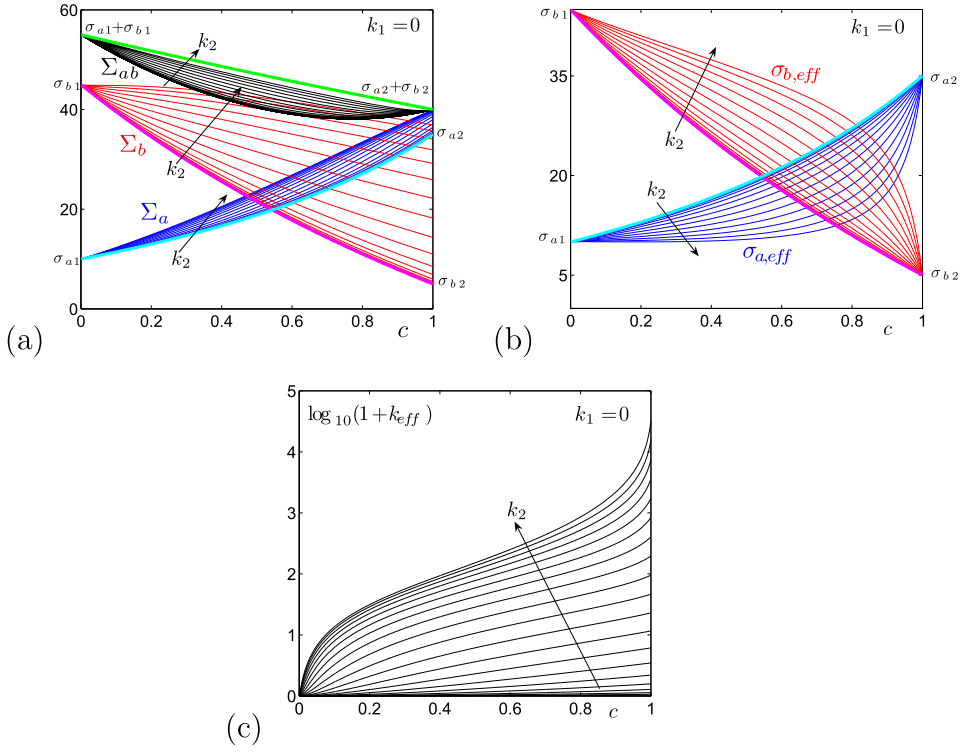

Fig. 6. Results for the composite sphere concerning the case with $k_1 = 0$ and $k_2 \neq 0$. We used 20 equispaced (in logarithmic scale) values of k_2 in the range $-1.5 < \log_{10} k_2 < 4.5$. We represented Σ_a, Σ_b and Σ_{ab} (a), $\sigma_{a,eff}$ and $\sigma_{b,eff}$ (b), and k_{eff} (c) versus $c = R_2^3/R_1^3$.

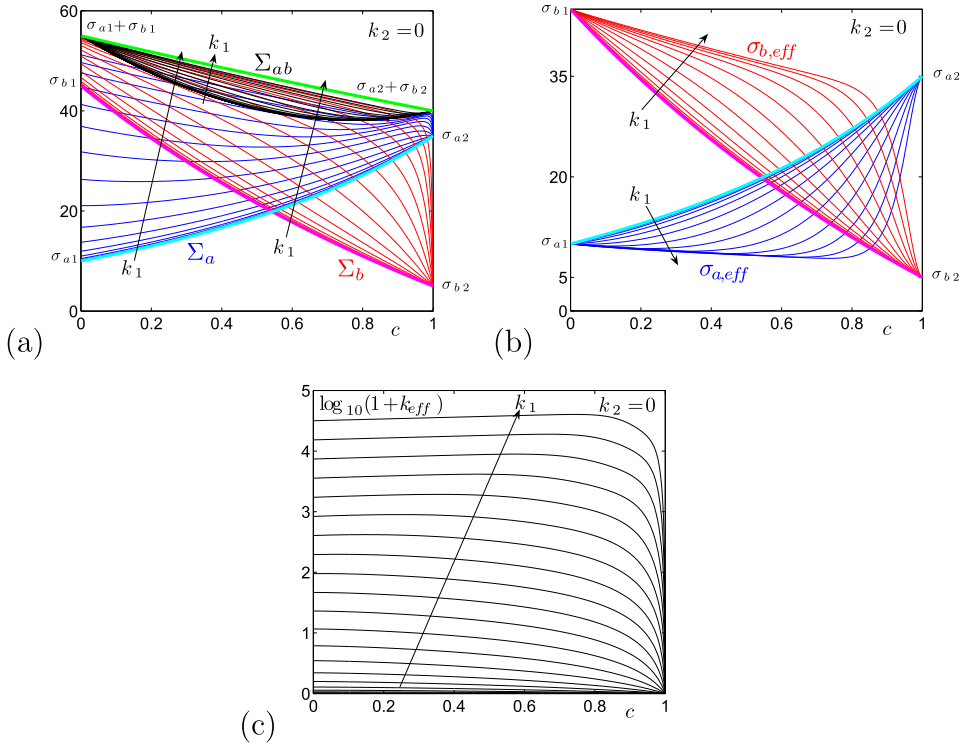

Fig. 7. Results for the composite sphere concerning the case with $k_1 \neq 0$ and $k_2 = 0$. We used 20 equispaced (in logarithmic scale) values of k_1 in the range $-1.5 < \log_{10} k_1 < 4.5$. We represented Σ_a, Σ_b and Σ_{ab} (a), $\sigma_{a,eff}$ and $\sigma_{b,eff}$ (b), and k_{eff} (c) versus $c = R_2^2/R_1^3$.

$$\sigma_{Max} = \sigma_1 \frac{2\sigma_1 + \sigma_2 - 2c(\sigma_1 - \sigma_2)}{2\sigma_1 + \sigma_2 + c(\sigma_1 - \sigma_2)} \tag{71}$$

where $c = R_2^3/R_1^3$, as before. This expression represents the exact effective Maxwell conductivity for a composite sphere with single-temperature behavior [5,8]. It is easy to realize that the structure of this expression is identical to Eqs. (66) and (67), indeed representing composite spheres where the coupling effects between the phases is removed, i.e. $k_1 = 0$ and $k_2 = 0$.

On the other hand, for k_1 or k_2 approaching infinity we observe a response defined by the Maxwell rule between two media having conductivities $\sigma_{t1} = \sigma_{a1} + \sigma_{b1}$ and $\sigma_{t2} = \sigma_{a2} + \sigma_{b2}$,

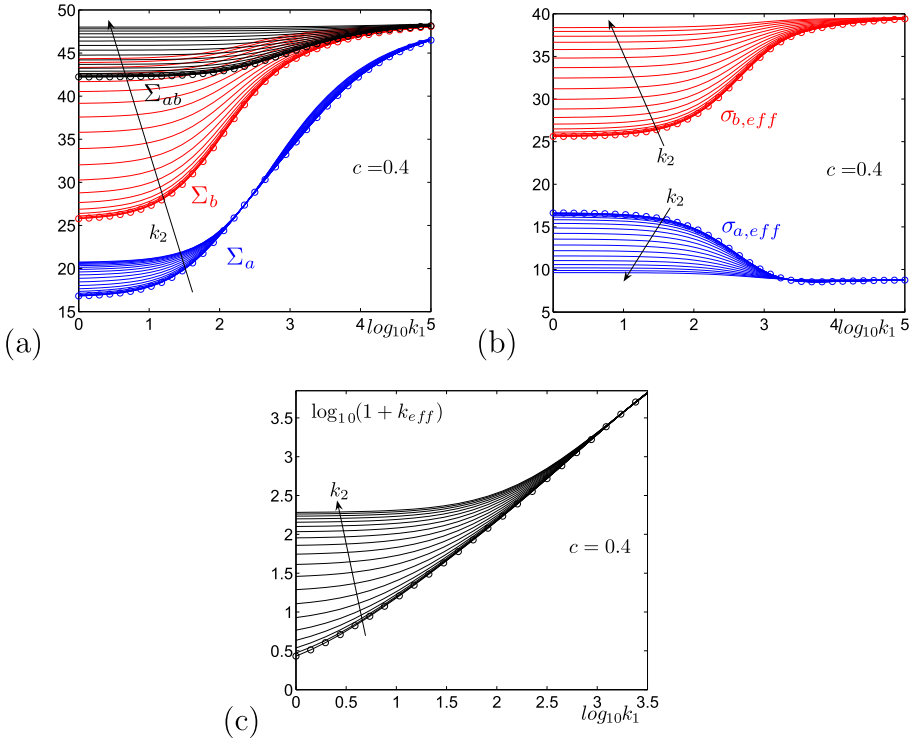

Fig. 8. Behavior of the composite sphere in terms of the coupling coefficients k_1 and k_2, for a fixed value of the volume fraction $c = 0.4$. The equivalent conductivities Σ_a, Σ_b and Σ_{ab} (a), the effective conductivities $\sigma_{a,eff}$ and $\sigma_{b,eff}$ (b), and the effective coupling parameter k_{eff} (c) are plotted versus k_1 and parametrized by k_2 (the circles correspond to the lowest value). We used 20 equispaced (in logarithmic scale) values of k_2 in the range $0 < \log_{10} k_2 < 5$.

$$\sigma_{Max,ab} = \sigma_{t1}\frac{2\sigma_{t1}+\sigma_{t2}-2c(\sigma_{t1}-\sigma_{t2})}{2\sigma_{t1}+\sigma_{t2}+c(\sigma_{t1}-\sigma_{t2})}, \tag{72}$$

represented by the heavy green curve in Figs. 6a and 7a. If $k_2 \to \infty$ we have Σ_{ab} converging to the value $\sigma_{Max,ab}$ while Σ_a and Σ_b converge to different curves not represented by any Maxwell rule (see Fig. 6a). Moreover, if $k_1 \to \infty$ all the three conductivities Σ_{ab}, Σ_a and Σ_b converge to the Maxwell value $\sigma_{Max,ab}$ (see Fig. 7a). It means that the condition $k_1 \to \infty, k_2 = 0$ is stronger than $k_2 \to \infty, k_1 = 0$, forcing all the three equivalent conductivities to be equal to the Maxwell value $\sigma_{Max,ab}$. The same behavior can be observed in Fig. 8a. We remark that the Maxwell relationships used in this discussion are exact for any value of the volume fraction c in the entire range $(0,1)$. This is true because of the simple geometry here considered, consisting in two concentric spheres. On the contrary, the original Maxwell rule is valid for small value of c, being conceived for a random dispersion of particles [5,8].

The results of the present Section can be summarized by stating the *second theorem of equivalence*: if we take into consideration a composite sphere formed by a two-temperature core and a two-temperature shell (i.e. described by six parameters $\sigma_{a2}, \sigma_{b2}, k_2, \sigma_{a1}, \sigma_{b1}$ and k_1) and embedded in an arbitrary two-temperature medium, then we can substitute the composite sphere with an homogeneous two-temperature sphere with parameters $\sigma_{a,eff}, \sigma_{b,eff}$ and k_{eff}, defined by the outlined procedure. It means that the thermal fields existing within the arbitrary two-temperature matrix (around the composite particle) are exactly the same before and after the formal substitution above introduced. The proof of this property can be sketched as follows. We consider these two different configurations:

- a composite sphere embedded in a given matrix, i.e. a system composed of three two-temperature materials subjected to a remotely applied temperature gradient. The problem can be easily solved (e.g., numerically or in a mathematical symbolic environment) by exploiting the general solution presented in Section 2;
- an homogeneous sphere embedded in a given matrix, i.e. a system composed of two phases subjected to a remotely applied temperature gradient. Of course, this homogeneous sphere is considered with the effective parameters discussed in the present Section, homogenizing the composite particle of the previous point. Such a problem has been exactly solved in Section 3.

We proved analytically and numerically that the external fields, for both situations, are exactly the same, thus confirming the above statement. We do not report here all the details of this calculation, which is very long but quite straightforward. Of course, as particular case we can consider a single-temperature description for the matrix, e. g. allowing the analysis of coated metal particles embedded in a dielectric matrix (see next Section). Importantly, as above said, the coating should be used to introduce the concepts of imperfect interface and mixing between electrons and phonons at the interface. To conclude, we also note that the above theorem of equivalence can be used iteratively for homogenizing an arbitrarily multi-coated two-temperature sphere (starting from the core and arriving at the most external shell). We remark that this iterative procedure is extremely more efficient than the standard one based on (i) considering the general solution given in Eqs. (22) and (23) for each phase and (ii) solving a very large system of equations for all the unknown coefficients. This point allows us to use such a methodology for graded structures, where it is important to consider a large number of shells to conveniently represent the continuously varying physical properties.

6. Dispersions of particles homogenization

In this Section, we consider a dispersion of identical double-conductivity particles dispersed in a single-temperature matrix. The aim is that of analysing the effects generated by a thin interphase between particles and matrix, mimicking the mixing phenomena and the imperfect transport properties. To do this,

the interphase will be considered as a two-temperature medium. Therefore, we adopt the model for two-temperature composite spheres introduced in Section 5. We suppose that the matrix medium is directly connected only to the phase a of the interphase. Hence, the particle (interphase + core) response is described by the equivalent thermal conductivity Σ_a, easily computable through Eq. (48), where ξ is obtained from Eq. (63). As a result, for a dilute mixture, we can apply the Maxwell [5] expression

$$\sigma_{eff} = \sigma_m \frac{2\sigma_m + \Sigma_a - 2\phi(\sigma_m - \Sigma_a)}{2\sigma_m + \Sigma_a + \phi(\sigma_m - \Sigma_a)}, \tag{73}$$

where σ_m is the conductivity of the matrix, ϕ is the volume fraction of the particles and Σ_a is their equivalent conductivity, which can be written in terms of the parameters describing the interphase/core thermal response

$$\Sigma_a = \Sigma_a(\sigma_{a2}, \sigma_{b2}, k_2, R_2, \sigma_{a1}, \sigma_{b1}, k_1, R_1). \tag{74}$$

Here, the radii R_1 and R_2 certainly fulfill the expression $R_2 = c^{1/3}R_1$, where c is the volume fraction of the core within the composite particle.

We remark that we used the Maxwell approach [5] (dilute limit) in order to obtain simple results and to directly analyse the effects induced by the two-temperature behavior and the imperfect interphases. Nevertheless, the quantity Σ_a discussed in Section 5 can be easily exploited to implement other homogenization techniques such as the differential method [8,24,71], the self consistent scheme [72–74], the generalized-self-consistent model [75] or the strong-property-fluctuation theory [21].

Anyway, here we study the system described by the combination of Eqs. (73) and (74). In Fig. 9 we analyse the effects of the imperfect contacts by plotting the overall effective conductivity σ_{eff} in terms of the interphase conductivity (for the sake of simplicity, we used $\sigma_{a1} = \sigma_{b1} \triangleq \sigma_1$) and of the mixing parameter k_1. First of all, we clarify the limits of the effective conductivity for very small and very large values of σ_1. To do this, we define the conductivity σ_0, which represents the value of the Maxwell expression given in Eq. (73) for $\Sigma_a \to 0$ (dispersion of voids), and the conductivity σ_∞, which characterizes a Maxwell dispersion for $\Sigma_a \to \infty$ (dispersion of superconducting particles),

$$\frac{\sigma_0}{\sigma_m} = \frac{2(1-\phi)}{2+\phi}, \quad \frac{\sigma_\infty}{\sigma_m} = \frac{1+2\phi}{1-\phi}. \tag{75}$$

Of course, we have that $\Sigma_a \to 0$ if $\sigma_1 \to 0$ and $\Sigma_a \to \infty$ if $\sigma_1 \to \infty$; therefore, the searched limiting behaviors are given by

$$\lim_{\sigma_1 \to 0} \sigma_{eff} = \sigma_0 = \sigma_m \frac{2(1-\phi)}{2+\phi}, \tag{76}$$

$$\lim_{\sigma_1 \to \infty} \sigma_{eff} = \sigma_\infty = \sigma_m \frac{1+2\phi}{1-\phi}. \tag{77}$$

It is not difficult to verify that these limits are in perfect agreement with the asymptotic behavior of any curve represented in Fig. 9 (dashed straight lines for $\sigma_1 \to \infty$ and dotted straight lines for $\sigma_1 \to 0$ in the left panel). In the left panel of Fig. 9 we show the behavior of σ_{eff} versus the properties of the interphase (σ_1 and k_1) for different values of ϕ and with a fixed value of c. Similarly, in the right panel, we show the same results with a varying c and a fixed ϕ. We have explored all the possible values of σ_1 ranging between the *low* and the *high* conducting interface model [33,37,39,43]. As a general conclusion, we observe that the effects induced by σ_1 (imperfect transport at the interfaces) are stronger than those generated by k_1 (mixing at the interfaces). Nevertheless, both aspect are important to define the overall behavior of the composite system: we remark that our procedure, based on the exact definition of Σ_a, is properly suited to consider an arbitrary two-temperature response for core and shell phases and, therefore, we can explore all the features of this heterogeneous structure. From Fig. 9 we also deduce that the volume fraction ϕ of the particles in the matrix strongly modifies the limits of σ_{eff} for small and large values of σ_1: see also Eqs. (76) and (77). On the other hand, the volume fraction c of the core within each particle does not modify these limits, while it slightly affects the threshold of σ_1 needed to obtain a given conductivity σ_{eff}.

To conclude this discussion, we show in Fig. 10 some results concerning the scale effects in heterogeneous two-temperature materials. In the left panel of Fig. 10 one can find the behavior of a dispersion of homogeneous double-conductivity spheres (without interphases, $R_1 = R_2$). It means that these results can be obtained through the combination of Eq. (73) with Eq. (49). The effective conductivity σ_{eff} is plotted versus the radius R_1 of the particles for different values of the coupling coefficients k_2. It is interesting to observe that σ_{eff} is an increasing function of R_1 and k_2. This behavior can be explained by observing that a larger particle allows to better exploit the conductivity of the phase b (disconnected from the matrix) through the parameter k_2 (note that no scale effects are present for $k_2 = 0$). In the right panel of Fig. 10 some scale effects are presented for a dispersion of composite particles (with interphase, $R_1 \neq R_2$). In this case Eqs. (73) and (74) have been utilised with varying R_1 and k_1, being fixed all the other parameters. Also this configuration exhibits an effective conductivity σ_{eff} that depends on R_1 (via an increasing function), with fixed values of c and ϕ, confirming the existence of relevant scale effects also in this case.

The proposed technique can be adopted to study complex porous media constituted by the following structure: we can consider a dispersion of particle composed of an arbitrary number of shell with a void or empty core. In this case we have a population of voids with an arbitrarily complicated two-temperature behavior

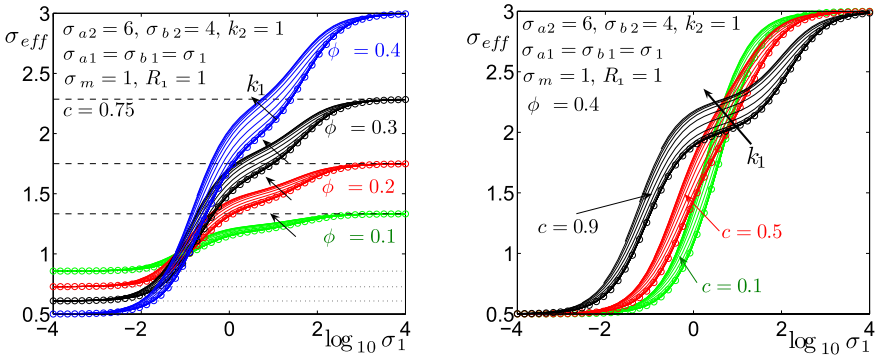

Fig. 9. Effective conductivity of a dispersion of two-temperature composite particles in terms of the conductivity of the interphase $\sigma_1 = \sigma_{a1} = \sigma_{b1}$ and the mixing parameter k_1. Left panel: four values of $\phi = 0.1, 0.2, 0.3, 0.4$ have been considered with a fixed $c = 0.75$. Right panel: three values of $c = 0.1, 0.5, 0.9$ were used with a fixed $\phi = 0.4$. In any family of curves we used 20 equispaced (in logarithmic scale) values of k_1 in the range $-4 < \log_{10} k_1 < 4$ (the circles correspond to the lowest value).

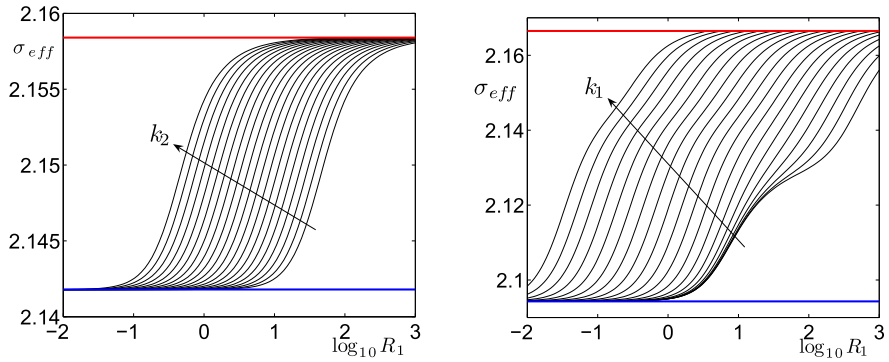

Fig. 10. Scale effects in a dispersion of homogeneous spheres (left) and composite spheres (right). In the left panel we have $R_1 = R_2$ (particle without interphase) and the effective conductivity σ_{eff} is represented versus R_1 and k_2 ($-2 < \log_{10} k_2 < 2, \sigma_{a2} = 35, \sigma_{b2} = 5, \sigma_m = 1, \phi = 0.3$). In the right panel we have $R_1 \neq R_2$ (particle with interphase) and the effective conductivity σ_{eff} is represented versus R_1 and k_1 ($-2 < \log_{10} k_1 < 5, k_2 = 1, \sigma_{a1} = 10, \sigma_{a2} = 35, \sigma_{b1} = 45$ and $\sigma_{b2} = 5, \sigma_m = 1, \phi = 0.3, c = 0.75$).

of the interphase between the pore and the matrix. However, the matrix must be considered with a single-temperature behavior in order to apply the proposed methodology. The case of saturated pores can be envisaged as well, with an arbitrary two-temperature behavior of the core. We can affirm that the consideration of a single-temperature behavior for the matrix is not a strong limitation since the more interesting and complicated effects occur in proximity of the heterogeneity of the system, the region that can be easily described by the two-temperature model. However, as above discussed, the limitations of our approach are mainly induced by the difficulties in treating transient, advection, source and non-linear terms.

7. Conclusions

In this paper we analysed heterogeneous materials or structures composed of phases described by the two-temperature model of heat conduction. More precisely, we considered and discussed some properties of the following configurations:

- we determined the behavior of a two-temperature sphere embedded in a two-temperature matrix: we pointed out that the scale effects depend on the relative size of the particle radius with respect to the parameters $1/h_i$ defined in Sections 2 and 3 (note that in the framework of the metal thermal conduction $1/h_i$ is named electron–phonon coupling length);
- we proved that a two-temperature sphere embedded in a single-temperature matrix can be substituted by an equivalent single-temperature particle having the conductivity obtained in Section 4. Moreover, we also showed that the knowledge of the three equivalent conductivities, obtained with the three different contact conditions between particles and matrix, is necessary and sufficient to have a complete characterization of the two-temperature particle response. This point is crucial for developing the following property;
- a composite sphere formed by a two-temperature core and a two-temperature shell, embedded in an arbitrary medium, can be substituted with an homogeneous two-temperature sphere with parameters defined by the procedure outlined in Section 5. This is an important feature for modeling complex interfaces (with mixing phenomena and imperfect transport) and graded or multi-coated structures.

Previous properties have been used to determine the effective behavior of a dilute dispersion of particles with complex interfaces. In particular, we firstly analysed the effects of geometrical aspects: (i) the thickness of the external layer mimicking the behavior of the interfaces (or, equivalently, the volume fraction c of the core within the shell) and (ii) the volume fraction ϕ of the particle dispersed in the matrix. Moreover, we investigated the influence of the physical interface features, i.e. (iii) the parameter k_1 describing the mixing phenomena between the phases a and b and (iv) the parameter σ_1 modulating the imperfect transport across the interface (exploring all the possibilities between the *low* and the *high* conducting interface). Although both physical parameters play an important role in defining the overall properties of the composite material, we observed that the effects induced by imperfect transport are generally stronger than those generated by the mixing at the interfaces. To conclude, we also remarked that the presence of two-temperature components induces relevant scale effects also in dispersions of particles. In this case, the overall response of the structure is characterized by well defined values of conductivities for very small or very large values of the particles radius, precisely identifying the nano- and the micro/macro-scale behaviors.

Conflict of Interest

None declared.

Appendix A. On the particular solution of the nonhomogeneous modified spherical Bessel equation

We search for the particular solution of the following nonhomogeneous differential equation

$$\frac{\mathrm{d}^2 V_{nm}}{\mathrm{d}r^2} + \frac{2}{r}\frac{\mathrm{d}V_{nm}}{\mathrm{d}r} - \left[n(n+1) + r^2 h^2\right]\frac{V_{nm}}{r^2} = f_{nm}, \tag{A.1}$$

where $f_{nm} = B_{nm} r^n + \frac{C_{nm}}{r^{n+1}}$ is the source term (see Eq. (15)). We apply the method of undetermined coefficients and we search V^{p}_{nm} in the form

$$V^{\mathrm{p}}_{nm} = C^{\mathrm{i}}_{nm}(r)\mathrm{i}_n(hr) + C^{\mathrm{k}}_{nm}(r)\mathrm{k}_n(hr). \tag{A.2}$$

This technique, as well known [76], simply leads to the following system for the unknown coefficients

$$\frac{\mathrm{d}C^{\mathrm{i}}_{nm}(r)}{\mathrm{d}r}\mathrm{i}_n(hr) + \frac{\mathrm{d}C^{\mathrm{k}}_{nm}(r)}{\mathrm{d}r}\mathrm{k}_n(hr) = 0, \tag{A.3}$$

$$\frac{\mathrm{d}C^{\mathrm{i}}_{nm}(r)}{\mathrm{d}r}\mathrm{i}'_n(hr) + \frac{\mathrm{d}C^{\mathrm{k}}_{nm}(r)}{\mathrm{d}r}\mathrm{k}'_n(hr) = \frac{1}{h} f_{nm}, \tag{A.4}$$

where $\mathrm{i}'_n(z) = \frac{\mathrm{d}}{\mathrm{d}z}\mathrm{i}_n(z)$ and $\mathrm{k}'_n(z) = \frac{\mathrm{d}}{\mathrm{d}z}\mathrm{k}_n(z)$. Since the Wronskian determinant of $\mathrm{i}_n(z)$ and $\mathrm{k}_n(z)$ is given by [69]

$$W(\mathrm{i}_n, \mathrm{k}_n) = \mathrm{i}_n(z)\mathrm{k}'_n(z) - \mathrm{i}'_n(z)\mathrm{k}_n(z) = -\frac{\pi}{2z^2}, \tag{A.5}$$

we simply obtain

$$V_{nm}^{\mathrm{p}} = \frac{2h}{\pi}\left[\int r^2 \mathrm{k}_n(hr) f_{nm}(r)\mathrm{d}r \mathrm{i}_n(hr) - \int r^2 \mathrm{i}_n(hr) f_{nm}(r)\mathrm{d}r \mathrm{k}_n(hr)\right]. \tag{A.6}$$

Moreover, since $f_{nm} = B_{nm}r^n + \frac{C_{nm}}{r^{n+1}}$ we analyse separately the two cases $f_{nm}^{(1)} = r^n$ and $f_{nm}^{(2)} = \frac{1}{r^{n+1}}$. By using Eq. (16) we can write the first particular solution as

$$V_{nm}^{\mathrm{p}(1)} = \frac{1}{r^{\frac{1}{2}}h^{n+\frac{5}{2}}}\left[\int w^{n+\frac{3}{2}} K_{n+\frac{1}{2}}(w)\mathrm{d}w I_{n+\frac{1}{2}}(hr) - \int w^{n+\frac{3}{2}} I_{n+\frac{1}{2}}(w)\mathrm{d}w K_{n+\frac{1}{2}}(hr)\right], \tag{A.7}$$

where we introduced the variable $w = hr$. We use the standard integrals [67]

$$\begin{aligned}
&\int w^{v+1} K_v(w)\mathrm{d}w = -w^{v+1}K_{v+1}(w) + C,\\
&\int w^{v+1} I_v(w)\mathrm{d}w = w^{v+1}I_{v+1}(w) + C,
\end{aligned} \tag{A.8}$$

and the following property of the Wronskian determinant for the modified cylindrical Bessel functions [69]

$$W(I_v, K_v) = I_v(z)K_{v+1}(z) + I_{v+1}(z)K_v(z) = \frac{1}{z} \tag{A.9}$$

for eventually obtaining

$$V_{nm}^{\mathrm{p}(1)} = -\frac{r^n}{h^2}. \tag{A.10}$$

Similarly, the second particular solution is given by

$$V_{nm}^{\mathrm{p}(2)} = \frac{1}{r^{\frac{1}{2}}h^{\frac{3}{2}-n}}\left[\int w^{\frac{1}{2}-n} K_{n+\frac{1}{2}}(w)\mathrm{d}w I_{n+\frac{1}{2}}(hr) - \int w^{\frac{1}{2}-n} I_{n+\frac{1}{2}}(w)\mathrm{d}w K_{n+\frac{1}{2}}(hr)\right] \tag{A.11}$$

where, as before, we have $w = hr$. We use now these standard integrals [67]

$$\begin{aligned}
&\int w^{1-v} K_v(w)\mathrm{d}w = -w^{1-v}K_{v-1}(w) + C,\\
&\int w^{1-v} I_v(w)\mathrm{d}w = w^{1-v}I_{v-1}(w) + C,
\end{aligned} \tag{A.12}$$

and Eq. (A.9) to obtain the second result

$$V_{nm}^{\mathrm{p}(2)} = -\frac{1}{h^2 r^{n+1}}. \tag{A.13}$$

To conclude, we can use Eqs. (A.10) and (A.13) in order to prove Eq. (20), representing the particular solution of the modified spherical Bessel equation.

References

[1] M. Sahimi, Heterogeneous materials I, in: Linear Transport and Optical Properties, Springer Verlag, New York, 2003.
[2] M. Sahimi, Heterogeneous materials II, in: Nonlinear and Breakdown Properties and Atomistic Modeling, Springer Verlag, New York, 2003.
[3] G.W. Milton, The Theory of Composites, Cambridge University Press, Cambridge, 2002.
[4] S. Torquato, Random Heterogeneous Materials, Springer Verlag, New York, 2002.
[5] J.C. Maxwell, A Treatise on Electricity and Magnetism, Clarendon Press, Oxford, 1881.
[6] H. Fricke, The Maxwell–Wagner dispersion in a suspension of ellipsoids, J. Phys. Chem. 57 (1953) 934.
[7] D.A.G. Bruggeman, Dielektrizitatskonstanten und Leitfahigkeiten der Mishkorper aus isotropen Substanzen, Ann. Phys. Leipzig 24 (1935) 636.
[8] S. Giordano, Effective medium theory for dispersions of dielectric ellipsoids, J. Electrostat. 58 (2003) 59.
[9] R. Günther, D. Heinrich, Dielektrizitätskonstante, Permeabilität, elektrische Leitfähigkeit, Wärmeleitfähigkeit und Diffusionskonstante von Gemischen mit kugelförmigen Teilchen (gitterförmige und statistische Anordnung), Z. Physik 185 (1965) 345.
[10] S. Giordano, Multipole analysis of a generic system of dielectric cylinders and application to fibrous materials, J. Electrostat. 63 (2005) 1.
[11] D.J. Bergman, O. Levy, D. Stroud, Theory of optical bistability in a weakly nonlinear composite medium, Phys. Rev. B 49 (1994) 129.
[12] P.M. Hui, P. Cheung, D. Stroud, Theory of third harmonic generation in random composites of nonlinear dielectrics, J. Appl. Phys. 84 (1998) 3451.
[13] L. Colombo, S. Giordano, Nonlinear elasticity in nanostructured materials, Rep. Prog. Phys. 74 (2011) 116501.
[14] S. Giordano, W. Rocchia, Shape dependent effects of dielectrically nonlinear inclusions in heterogeneous media, J. Appl. Phys. 98 (2005) 104101.
[15] S. Giordano, W. Rocchia, Predicting dielectric nonlinearity of anisotropic composite materials via tensorial analysis, J. Phys.: Condens. Matter. 18 (2006) 10585.
[16] H. Hatta, M. Taya, Equivalent inclusion method for steady state heat conduction in composites, Int. J. Eng. Sci. 24 (1986) 1159.
[17] H. Hatta, M. Taya, Effective thermal conductivity of a misoriented short fiber composite, J. Appl. Phys. 58 (1985) 2478.
[18] H. Hatta, M. Taya, Thermal conductivity of coated filler composites, J. Appl. Phys. 59 (1986) 1851.
[19] W.S. Weiglhofer, A. Lakhtakia, B. Michel, Maxwell–Garnett and Bruggeman formalisms for a particulate composite with bianisotropic host medium, Microwave Opt. Technol. Lett. 15 (1997) 263.
[20] A. Lakhtakia, W.S. Weiglhofer, Maxwell–Garnett formalism for weakly nonlinear, bianisotropic, dilute, particulate composite media, Int. J. Electron. 87 (2000) 1401.
[21] Tom G. Mackay, Effective constitutive parameters of linear nanocomposites in the long-wavelength regime, J. Nanophotonics 5 (2011) 051001.
[22] A. Akbari, M. Akbari, R.J. Hill, Effective thermal conductivity of two-dimensional anisotropic two-phase media, Int. J. Heat Mass Transfer 63 (2013) 41.
[23] S. Giordano, P.L. Palla, Dielectric behavior of anisotropic inhomogeneities: interior and exterior points Eshelby tensors, J. Phys. A: Math. Theor. 41 (2008) 415205.
[24] S. Giordano, P.L. Palla, Conduction degradation in anisotropic multi-cracked materials, Eur. Phys. J. B 85 (2012) 59.
[25] P.H.M. Böttger, A.V. Gusarov, V. Shklover, J. Patscheider, M. Sobiech, Anisotropic layered media with microinclusions: thermal properties of arc-evaporation multilayer metal nitrides, Int. J. Therm. Sci. 77 (2014) 75.
[26] A.P. Wemhoff, Thermal conductivity predictions of composites containing percolated networks of uniform cylindrical inclusions, Int. J. Heat Mass Transfer 62 (2013) 255.
[27] J.-L. Auriault, Wave propagation and transient heat transfer in thermoelastic composites, Int. J. Heat Mass Transfer 55 (2012) 5972.
[28] W. Evans, R. Prasher, J. Fish, P. Meakin, P. Phelan, P. Keblinsky, Effect of aggregation and interfacial thermal resistance on thermal conductivity of nanocomposites and colloidal nanofluids, Int. J. Heat Mass Transfer 51 (2008) 1431.
[29] P.L. Kapitza, Collected Papers of P.L. Kapitza, vol. 3, Pergamon Press, Oxford, 1964–1967.
[30] Y. Benveniste, T. Miloh, The effective conductivity of composites with imperfect thermal contact at constituent interfaces, Int. J. Eng. Sci. 24 (1986) 1537.
[31] Y. Benveniste, Effective thermal conductivity of composites with a thermal contact resistance between the constituents: nondilute case, J. Appl. Phys. 61 (1987) 2840.
[32] D.P.H. Hasselman, L.F. Johnson, Effective thermal conductivity of composites with interfacial thermal barrier resistance, J. Compos. Mater. 21 (1987) 508.
[33] S. Torquato, M.D. Rintoul, Effect of the interface on the properties of composite media, Phys. Rev. Lett. 75 (1995) 4067.
[34] R. Lipton, B. Vernescu, Critical Radius, Size effects and extremal microgeometries for composites with imperfect interface, J. Appl. Phys. 79 (1996) 8964.
[35] C.-W. Nan, R. Birringer, D.R. Clarke, H. Gleiter, Effective thermal conductivity of particulate composites with interfacial thermal resistance, J. Appl.Phys. 81 (1997) 6692.
[36] Z. Hashin, Thin interphase/imperfect interface in conductivity, J. Appl. Phys. 89 (2001) 2261.
[37] H.L. Duan, B.L. Karihaloo, Effective thermal conductivities of heterogeneous media containing multiple imperfectly bonded inclusions, Phys. Rev. B 75 (2007) 064206.
[38] H. Le Quang, Q.-C. He, G. Bonnet, Eshelby's tensor fields and effective conductivity of composites made of anisotropic phases with Kapitza's interface thermal resistance, Philos. Mag. 91 (2011) 3358.
[39] H. Le Quang, D.C. Pham, G. Bonnet, Q.-C. He, Estimations of the effective conductivity of anisotropic multiphase composites with imperfect interfaces, Int. J. Heat Mass Transfer 58 (2013) 175.
[40] R. Lipton, Variational methods, bounds, and size effects for composites with highly conducting interface, J. Mech. Phys. Solids 45 (1997) 361.
[41] T. Miloh, Y. Benveniste, On the effective conductivity of composites with ellipsoidal inhomogeneities and highly conducting interfaces, Proc. R. Soc. London, Ser. A455 (1999) 2687.
[42] H. Le Quang, G. Bonnet, Q.-C. He, Size-dependent Eshelby tensor fields and effective conductivity of composites made of anisotropic phases with highly conducting imperfect interfaces, Phys. Rev. B 81 (2010) 064203.
[43] F. Pavanello, F. Manca, P.L. Palla, S. Giordano, Generalized interface models for transport phenomena: Unusual scale effects in composite nanomaterials, J. Appl. Phys. 112 (2012) 084306.
[44] F. Pavanello, S. Giordano, How imperfect interfaces affect the nonlinear transport properties in composite nanomaterials, J. Appl. Phys. 113 (2013) 154310.

[45] Y. Benveniste, Models of thin interphases and the effective medium approximation in composite media with curvilinearly anisotropic coated inclusions, Int. J. Eng. Sci. 72 (2013) 140.
[46] M.I. Kaganov, I.M. Lifshitz, L.V. Tanatarov, Relaxation between electrons and the crystalline lattice, Sov. Phys. JETP 4 (1957) 173–178 [Zh. Eksp. Teor. Fiz. 31 232–237 (1956)]..
[47] S.I. Anisimov, B.L. Kapeliovich, T.L. Perelman, Electron emission from metal surfaces exposed to ultrashort laser pulses, Sov. Phys. JETP 39 (1974) 375–377 [Zh. Eksp. Teor. Fiz. 66 776–781 (1974)]..
[48] H.E. Elsayed-Ali, T.B. Norris, M.A. Pessot, G.A. Mourou, Time-resolved observation of electron-phonon relaxation in Copper, Phys. Rev. Lett. 58 (1987) 1212.
[49] P.B. Allen, Theory of thermal relaxation of electrons in metals, Phys. Rev. Lett. 59 (1987) 1460.
[50] A. Majumdar, P. Reddy, Role of electron–phonon coupling in thermal conductance of metal–nonmetal interfaces, Appl. Phys. Lett. 84 (2004) 4768.
[51] P. Singh, M. Seong, S. Sinha, Detailed consideration of the electron–phonon thermal conductance at metal–dielectric interfaces, Appl. Phys. Lett. 102 (2013) 181906.
[52] Y. Wang, X. Ruan, A.K. Roy, Two-temperature nonequilibrium molecular dynamics simulation of thermal transport across metal–nonmetal interfaces, Phys. Rev. B 85 (2012) 205311.
[53] C.L. Phillips, P.S. Crozier, An energy-conserving two-temperature model of radiation damage in single component and binary Lennard–Jones crystals, J. Chem. Phys. 131 (2009) 074701.
[54] D.A. Nield, A. Bejan, Convection in Porous Media, Springer Verlag, New York, 2006.
[55] J.L. Auriault, P. Royer, Double conductivity media: a comparison between phenomenological and homogenization approaches, Int. J. Heat Mass Transfer 36 (1993) 2613.
[56] M. Quintard, M. Kaviany, S. Whitaker, Two-medium treatment of heat transfer in porous media: numerical results for effective properties, Adv. Water Resour. 20 (1997) 77.
[57] A. Nouri-Borujerdi, A.R. Noghrehabadi, D.A.S. Rees, The effect of local thermal non-equilibrium on impulsive conduction in porous media, Int. J. Heat Mass Transfer 50 (2007) 3244.
[58] A. d'Hueppe, M. Chandesris, D. Jamet, B. Goyeau, Coupling a two-temperature model and a one-temperature model at a fluid-porous interface, Int. J. Heat Mass Transfer 55 (2012) 2510.
[59] Y. Davit, B.D. Wood, G. Debenest, M. Quintard, Correspondence between one- and two-equation models for solute transport in two-region heterogeneous porous media, Transp. Porous Media 95 (2012) 213.
[60] J. Ordonez-Miranda, J.J. Alvarado-Gil, R. Yang, The effect of the electron–phonon coupling on the effective thermal conductivity of metal–nonmetal multilayers, J. Appl. Phys. 109 (2011) 094310.
[61] J. Ordonez-Miranda, J.J. Alvarado-Gil, R. Yang, Effect of the electron–phonon coupling on the effective thermal conductivity of metallic bilayers, Int. J. Thermophys. 34 (2013) 1817.
[62] J. Ordonez-Miranda, J.J. Alvarado-Gil, R. Yang, A model for the effective thermal conductivity of metal–nonmetal particulate composites, J. Appl. Phys. 111 (2012) 044319.
[63] P. Vadasz, On the paradox of heat conduction in porous media subject to lack of local thermal equilibrium, Int. J. Heat Mass Transfer 50 (2007) 4131.
[64] L. Wang, X. Wei, Equivalence between dual-phase-lagging and two-phase-system heat conduction processes, Int. J. Heat Mass Transfer 51 (2008) 1751.
[65] L. Wang, X. Zhou, X. Wei, Heat Conduction: Mathematical Models and Analytical Solutions, Springer Verlag, Berlin, 2008.
[66] A. Prosperetti, Advanced Mathematics for Applications, Cambridge University Press, Cambridge, 2011.
[67] I.S. Gradshteyn, I.M. Ryzhik, Table of Integrals, Series and Products, Academic Press, San Diego, 1965.
[68] M. Abramowitz, I.A. Stegun, Handbook of Mathematical Functions, Dover Publication, New York, 1970.
[69] F.W.J. Olver, D.W. Lozier, R.F. Boisvert, C.W. Clark, NIST Handbook of Mathematical Functions, National Institute of Standards and Technology and Cambridge University Press, New York, 2010.
[70] S. Giordano, Order and disorder in the microstructure of dielectrically nonlinear heterogeneous materials, J. Electrostat. 68 (2010) 227.
[71] B. Michel, A. Lakhtakia, W.S. Weiglhofer, T.G. Mackay, Incremental and differential Maxwell Garnett formalisms for bi-anisotropic composites, Compos. Sci. Technol. 61 (2001) 13.
[72] A. Lakhtakia, Incremental Maxwell Garnett formalism for homogenizing particulate composite media, Microwave Opt. Technol. Lett. 17 (1998) 276.
[73] S. Giordano, Two-dimensional disordered lattice networks with substrate, Physica A 375 (2007) 726.
[74] S. Giordano, Relation between microscopic and macroscopic mechanical properties in random mixtures of elastic media, J. Eng. Mater. Technol. 129 (2007) 453.
[75] R.M. Christensen, K.H. Lo, Solutions for effective shear properties in three phase sphere and cylinder models, J. Mech. Phys. Solids 27 (1979) 315.
[76] L.S. Pontryagin, Ordinary Differential Equations, Addison-Wesley, New York, 1962.